Oxidation of Ethanol and Hydrocarbon Mixtures in a Pressurised Flow Reactor

Hao Yuan[a], Zhewen Lu[a], Zhongyuan Chen[a], Yi Yang[a,*], Michael J. Brear[a], James E. Anderson[b], Thomas Leone[b]

[a] *Department of Mechanical Engineering, The University of Melbourne, Parkville, Victoria 3010, Australia*
[b] *Ford Research and Advanced Engineering, Ford Motor Company, Dearborn, Michigan 48121, USA*

Abstract

This paper presents a study of the oxidation of iso-octane, ethanol, toluene and their mixtures in a pressurised turbulent flow reactor operating at 900-930 K, 10 bar, and an equivalence ratio of 0.058. A large set of fuels is investigated, including neat iso-octane, ethanol, toluene, their binary mixtures, gasoline reference fuels (PRF91 and TRF91), and their mixtures with ethanol. The resulting species are measured along the length of the reactor and simulated using existing kinetic models from the literature.

The existing models are found to reproduce measurements of the major oxidation products of iso-octane, ethanol, their binary mixtures, as well as that of PRF91 and PRF91/ethanol mixtures. However, significant differences are observed between the measurement and simulation of neat toluene. Adjustment is then made to the rate constants of key reactions in the toluene model. The adjusted model, whilst more accurately reproducing neat toluene oxidation, does not significantly improve the modelling of toluene containing mixtures. This suggests that further investigations should focus on the oxidation of neat toluene, as well as the chemical interactions of toluene containing mixtures.

Keywords:

Hydrocarbon Oxidation Chemistry, Flow Reactor, Ethanol, Toluene, Chemical Interactions

1. Introduction

Oxidation chemistry of gasoline is closely related to knock in spark-ignition (SI) engines and to the octane rating of gasoline fuels. Gasoline is comprised of hundreds of hydrocarbons of different types and also typically contains ethanol in many countries. Increased ethanol content has been investigated [1–3] due to the excellent anti-knock

*Corresponding author
Email address: yi.yang@unimelb.edu.au (Yi Yang)

properties and production routes from renewable sources. All these compounds differ in oxidation chemistry, and when blended together for practical use, can interact significantly during oxidation. This is evidenced by recent studies that reported highly non-linear blending behaviours in the octane number of ethanol/hydrocarbon mixtures [4, 5], in which super-linear (synergistic) blending was observed for ethanol/paraffins mixtures and sub-linear (antagonistic) blending was observed for ethanol/aromatic mixtures. Whereas correlations have been proposed to quantify these non-linear blending behaviours [6, 7], chemistry producing such blending has not been fully understood. This paper represents a first part of the effort to investigate this topic which studies the oxidation chemistry of a comprehensive set of fuels, including neat compounds and simple mixtures of these compounds, in a pressurised flow reactor. This paper also evaluates the kinetic models in the literature that have been proposed to simulate the oxidation of the fuels studied.

In the following, state of the art of kinetic models are first reviewed for the neat fuel compounds of interest to this work. A more detailed review is followed for fuel mixtures containing two and more components.

Iso-octane and n-heptane are the two reference compounds that are blended to produce primary reference fuels (PRF) and define the octane number scale for gasoline. They are also commonly used to represent branched alkanes and straight-chain alkanes in combustion chemistry research. Comprehensive kinetic models of iso-octane [8] and n-heptane [9] were first reported by Curran et al. and have undergone several updates, including that in the gasoline surrogate model by Mehl et al. [10], and more recently by Zhang et al. for n-heptane [11] and by Atef et al. for iso-octane [12]. These updates improved the sub-models of C_0-C_4 chemistry, refined the thermochemistry database, optimised the rate constants for selected reactions, and added new reaction pathways. New experimental data, in particular, ignition delays from shock tubes and rapid compression machines (RCM) and species concentrations from jet stirred reactors (JSR), were used to validate these updates.

Toluene is commonly referred as the representative compound of aromatics and has been extensively studied for the combustion chemistry. Kinetic models of toluene have been developed using data obtained from Princeton flow reactor in the past few decades [13–15]. The recent comprehensive model by Metcalfe et al. [15] was validated against a wide range of experiments, including flow reactor, shock tube, jet-stirred reactor, and flame studies. They also included new flow reactor data at 450-950 K, 12.5 atm., and various residence times and equivalence ratios. Yuan

et al. [16, 17] conducted experiment on toluene pyrolysis in a laminar flow reactor at 1 bar, and on toluene oxidation in a JSR at 10 bar. They updated a low pressure toluene model [18] from their own group by incorporating theoretical calculations for a number of key reactions. More recently, Zhang et al. [19] found that the existing toluene models could not reproduce the ignition delay measured in their shock tube and RCM at 624-1459 K and 20-40 bar. They subsequently revised an alkylbenzene model from Lawrence Livermore National Laboratory [20] (originally from Metcalfe et al. [15]) by adding new reaction classes and updating the rate constants of several key reactions. The revised model was found to better reproduce the ignition delay measurements. More recently, Pelucchi et al. [21] improved the models of Yuan et al.[16, 17] and Zhang et al. [19] by incorporating new rate constants from theoretical calculations on reactions involving toluene and benzyl radical.

As the most widely used biofuel, ethanol has been extensively studied for its oxidation chemistry. An early comprehensive kinetic model was developed by Marinov [22], which was improved in the subsequent development. Li et al. [23] updated this model using data of ethanol pyrolysis at 1045-1080 K and 1.7-3.0 atm. and ethanol oxidation at 800-950 K and 3-12 atm. in the Princeton flow reactor. Dagaut and Togbé [24] improved the Marinov model by including theoretical calculations for the first H-abstraction on ethanol [25–28] and validating with experiment in a JSR at 770-1220 K and 10 atm. Mittal et al. [29] further validated the Marinov model using RCM ignition delay data at 825-985 K and 10-50 bar. An independent development was reported by Leplat et al. [30] who proposed an ethanol model based on the species measurement from a laminar flame at 0.05 bar and a JSR at 890-1250 K and 1 atm.

Besides neat compounds, mixtures of varying complexity have been investigated. A major focus of these studies is the chemical interactions between fuel components during oxidation. PRF mixtures have been studied for their unique pertinence to octane rating. Dagaut et al. [31] studied a wide range of PRF mixtures in a JSR at 550-1150 K and 10 atm. and reported that the CO molar fraction, an indicator of oxidation reactivity, increased non-linearly with the blending level. Lu et al. [32] studied PRF mixtures from PRF0 (n-heptane) to PRF100 (iso-octane) in a flow reactor at 550-900 K and 10 bar, where they reported a linear relation between CO formation and the blending ratio. They further analysed the CO formation in a JSR [31] and a motored engine [33], as well as the ignition delays in shock tubes [34, 35], as a function of the blending ratio. They argued that the linear blending is generally applicable during the low temperature oxidation of PRFs when the temperature is < 900 K, therefore suggesting little interaction

between iso-octane and n-heptane at these conditions. A similar argument was also made by Wilk et al. [36] on the oxidation of PRFs (up to PRF25) from their flow reactor experiments.

Mixtures involving other hydrocarbon groups have also been investigated, and significant kinetic interactions have been reported in these cases. For example, Vanhove et al. [37] measured the ignition delay of the binary mixtures of iso-octane, 1-hexene, and toluene in a RCM at 600-900 K and 3-15 bar. The lack of linear correlation between the ignition delay and blending ratio led to the speculation that these compounds should interact via a shared radical pool during oxidation. Yahyaoui et al. [38] measured the ignition delay of 1-hexene/toluene mixtures in a shock tube at 1360-1860 K, 2-10 bar and determined the species concentrations of these mixtures in a JSR at 750-1170 K and 10 bar. From kinetic modelling, they argued that the chemical interactions between 1-hexene and toluene could involve both the radical pool and cross reactions of fuel-like species. Di Sante [39] studied the autoignition of n-heptane/toluene mixtures in a RCM at 710-840 K and 7.95-10.38 bar. They reported that the ignition delay increased only slightly with 25 vol% toluene added into n-heptane, indicating that the inhibiting effect of toluene on the autoignition is disproportionally low and thus the interaction between the two compounds was non-linear with respect to the blending ratio.

Significant interactions between ethanol and hydrocarbons have also been reported. Dagaut et al. [40–42] measured the species profiles from the oxidation of ethanol/n-heptane and ethanol/iso-octane mixtures in a JSR at 530-1190 K and 10 atm., where ethanol showed a strong inhibition effect on CO formation disproportional to the blending ratio. The strong inhibition effect of ethanol was also reported by Lu et al. [32] in ethanol/iso-octane mixtures in a flow reactor at 550-900 K and 10 bar, which was attributed by the authors to the super-linear octane blending between the two compounds [4]. Haas et al. [43] modelled the oxidation of ethanol/n-heptane mixtures in a flow reactor at 523-903 K and 12.5 atm. and discussed that ethanol consumed the OH radicals produced by n-heptane and converted it to less reactive HO2, thus reducing the overall reactivity of the mixture.

Fuel mixtures containing more than two compounds have also been studied [44–47]. These studies have generally focused on developing surrogate fuels. Chemical interactions are more complicated in these mixtures, but have rarely been explored. Nevertheless, kinetic models have been developed for these more complex mixtures, as recently reviewed by Sarathy et al. [48], using the conventional method that combines the sub-models of individual compounds

used to formulate the surrogate. The gasoline surrogate model by Mehl el al. [10] is an important contribution in this regard, and was created by combining the kinetic models of iso-octane, n-heptane, toluene, and 1-hexene, and then validating the mixture model against a large experimental dataset including ignition delay times, laminar flame speeds, and species data from JSR. This model was found to also perform reasonably well in reproducing ignition delay data later reported in [44–47]. A different approach was taken by Dooley et al. [49–51] who used group additivity theory [52] to formulate surrogate fuels based on the composition of molecular functional groups instead of hydrocarbon classes. This approach was successfully applied to the development of jet fuel surrogates, although the effectiveness of the method still relies on accurate modelling of the selected compounds that contain the functional groups for the surrogate formulation.

Despite these efforts, it is noted that the recent experimental investigations are composed mostly of ignition delays from shock tubes and RCMs, as well as species concentrations from JSR, whereas results from flow reactors are rarely reported. For example, flow reactor data were not used in updating the recent models for iso-octane [12] and n-heptane [11]. Flow reactor experiments characterise species evolution along the reaction progress which is valuable for understanding detailed reaction chemistry and validating comprehensive kinetic models. This study, therefore, uses a flow reactor and conducts a systematic investigation on the oxidation chemistry of neat fuels and fuel mixtures containing various numbers of components. The measured speciation data are used to evaluate the state of the art kinetic models available in the literature.

2. Experimental and Numerical Methods

2.1. Flow reactor facility

The experimental investigation is conducted in a pressurised, turbulent flow reactor recently built in the University of Melbourne. A schematic of the facility is shown in Fig. 1. Details of the reactor design and validation have been reported in [53], and a brief summary is therefore provided here. The reactor is a quartz tube of 25 mm diameter and 1000 mm length, housed in a pressure vessel rated at 50 bar at 1000 K. The fuel and air are preheated separately before entering the reactor. Air is supplied in large excess to reduce the reaction rate and allow gas sampling with fine spatial resolution in the reaction zone. Nitrogen is not used as the dilution gas due to its relatively high cost at the

required flow rates, and an oil-free compressor is used to pressurise the air. After the moisture is removed by a dryer, the air is heated to the required reaction temperature by an 8 kW in-line heater before entering the reactor. Inside the pressure vessel, the quartz tube is surrounded by three cylindrical heaters designed to minimise heat loss. A fraction of the compressed air flows in between the quartz tube and pressure vessel to minimise the pressure difference across the quartz wall. Liquid fuels are supplied from a fuel tank pressurised by nitrogen and are vaporised with nitrogen heated to 520 K. The air flow rate is controlled by a needle valve and measured by an in-line flow meter. The fuel flow rate is measured by a Coriolis flow meter and verified by temporal measurements of the weight of the fuel tank with a strain gauge. The vaporised fuel and hot air mix rapidly via a novel, orifice-plate mixer at the inlet of the reactor. Fast mixing was confirmed by injecting carbon dioxide from the fuel channel at 900 K and 10 bar, where the complete CO_2/air mixing was found to achieve at approximately 50 mm downstream of the mixer. The reactor pressure is controlled by a back pressure valve on the exhaust line.

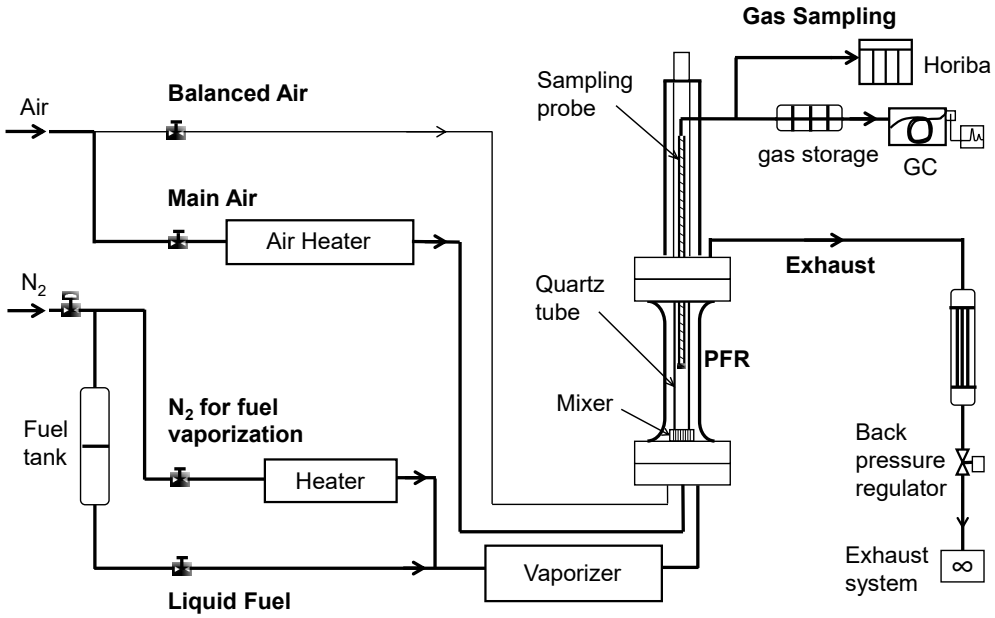

Figure 1: Schematic of the pressurised flow reactor system.

A water cooled sample probe at approximately 330 K is installed on a linear actuator for collecting gas samples along the centreline of the reactor. The sample probe is equipped with three K-type thermocouples of different sizes (0.27, 0.80, and 0.94 mm mean diameter) for gas temperature measurement. This novel method exploits the differing radiative losses of each thermocouple and the axisymmetric setup of the reactor and thermocouples. Using this

method, the temperature profile along the reactor centreline is obtained at each test condition without having to rely on assumed values for wall emissivity and convection heat transfer coefficients. Details of the temperature correction is provided in [53]. The uncertainty of the corrected temperature is estimated to be ±5 K at 900 K.

The sampled gas is transferred via a heated line (at 473 K) to a Horiba emission bench for CO and CO_2 measurement using non-dispersive infrared (NDIR) analysers. The measurement accuracy is 1% with a resolution of 20 ppm for CO and 30 ppm for CO_2. Alternatively, the sampled gas is sent to a Shimadzu gas chromatography (GC) for analysis of the fuel and intermediate species. Heated storage loops are used to temporarily store the samples before GC analysis. The GC is equipped with a fused silica PLOT column and a flame ionisation detector (FID). A multi-component gas standard is used for analysis of small hydrocarbons (C_1-C_4). Higher-boiling species are identified with liquid standards which are pre-vaporised and injected into the GC using the same method as the samples. Effective carbon numbers from the literature [54, 55] are used to quantify the FID peak area for the high-boiling species. Only major intermediate species that are well separated are reported in this work, for which the measurement uncertainties are $\leq$ 10%. Figure 2 shows a typical carbon balance along the reactor during the oxidation of iso-octane. Approximately 95% of the fuel carbon is accounted for over the first 400 mm, dropping to 70% as more intermediate species are formed. Not all intermediate species are analysed, including formaldehyde which has no response to the FID and those corresponding to various small, unidentified peaks on the GC spectra. Near the end of the reactor, most intermediates are converted to CO which brings the carbon balance above 80%. Details of the GC analysis can be found in [56].

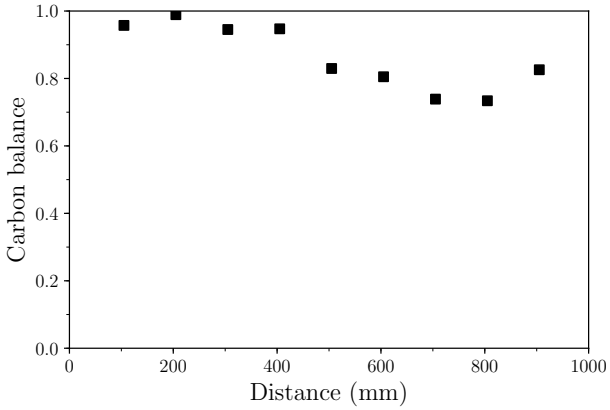

Figure 2: Carbon balance of iso-octane oxidation at 900 K, 10 bar, and ϕ=0.058

The reactor conditions have been validated against turbulent, plug-flow assumptions [53]. The flow inside the reactor is confirmed to be essentially isobaric and nearly adiabatic, with uniform radial profiles established at approximately 5-7% of the reactor length from the mixer. Negligible axial diffusion is confirmed by the Peclet number (diffusion time scale vs. advection time scale) of 100 calculated using the method in [57]. Wall reaction, such as catalytic decomposition of ethanol to ethylene and water [43], was not observed for the fuels tested.

2.2. Experimental conditions

Experimental conditions used in this work are shown in Table 1. Test fuels are shown in Table 2. All fuels were tested at 10 bar and 900 K except for neat toluene which was tested at 930 K due to the lower reactivity. The temperature of 900 K is used to represent the temperature at autoignition during the Research Octane Number (RON) test in the Cooperative Fuel Research engine [58]. The nominal temperature of the reactor is measured at the location of the mixer (0 mm of the reactor length). A fixed air flow rate is used, which yields a residence time of 0.27 s at 900 mm of the reactor. A constant equivalence ratio of 0.058 is used for all fuels tested. Due to the added nitrogen for fuel vaporisation, O_2 is 19.6-19.7% in the reactant mixture. Despite the low equivalence ratio, the fuel mole fraction in the starting mixture is similar to those using stoichiometric, N_2-diluted experiments [15, 59]. All experimental data of this work are provided in the Supplementary Information.

Table 1: Experimental conditions for the pressurised flow reactor study.

Reactor parameter	Set value
Reactor pressure (bar)	10
Reactor nominal temperature (K)[a]	900[b]
Equivalence ratio	0.058
Air flow rate (g/s)	6
Nitrogen flow rate (g/s)	0.32
Reynolds number in the reactor tube	8000
Fuel/nitrogen pressure (bar)	20-21
Fuel/nitrogen temperature (K)	500
Total residence time (s)	0.27

[a] The temperature is measured at the location of the mixer
[b] Neat toluene is tested at 930 K

2.3. Kinetic modelling method

The kinetic modelling uses a zero-dimensional, constant-pressure, plug-flow model in Chemkin-Pro [60]. Table 2 lists the kinetic models used in this work, which include some widely used in the literature and their recent updates. Instead solving the energy equation, the calculation uses the temperature profile determined with the 3-thermocouple method as an input to the model. Due to the fast mixing in the reactor, no time shift is required in the simulation [61].

Table 2: Test fuels and reaction models for modelling.

Fuel	model
Neat fuels	
iso-octane	Atef et al. [12] Mehl et al. [10] Andrae [62]
Ethanol	AramcoMech 2.0 [63] Mittal et al. [29] Mehl et al., 2011 [10] Andrae [62]
Toluene	Metcalfe et al. [15] Yuan et al. [16] Mehl et al. [10] Zhang et al. [19] Pelucchi et al. [21] Andrae [62]
Binary mixtures	
iso-octane/ethanol 26.1/73.9, 58.6/41.4, 76.1/23.9 by mole 50/50, 80/20, 90/10 by volume	Mehl et al. [10]
iso-octane/toluene 25/75, 50/50, 75/25 by mole 34.1/65.9, 60.8/39.2, 82.3/17.7 by volume	Mehl et al. [10] Mehl Adjusted[a]
ethanol/toluene 25/75, 50/50, 75/25 by mole 15.4/84.6, 35.4/64.6, 62.2/37.8 by volume	Mehl et al. [10] Mehl Adjusted'
Gasoline surrogates	
PRF91: iso-octane/n-heptane 90/10 by mole 91/9 by volume	Mehl et al. [10]
[b] TRF91-30: iso-octane/n-heptane/toluene 44.9/16.2/38.9 by mole 53.2/17.0/29.8 by volume	Mehl et al. [10] Mehl Adjusted
Gasoline surrogates and ethanol	
PRF91 and ethanol: iso-octane/n-heptane/ethanol 23.7/2.6/73.7 by mole 45.5/4.5/50.0 by volume	Mehl et al. [10]
TRF91-30 and ethanol: iso-octane/n-heptane/toluene/ethanol 13.3/4.8/11.5/70.4 by mole 26.6/8.5/14.9/50.0 by volume	Mehl et al. [10] Mehl Adjusted

[a] Mehl Adjusted is from this work revised from Mehl et al. [10] (details provided later in this paper)
[b] TRF is toluene reference fuel

3. Results and Discussion

3.1. Neat fuels

3.1.1. Iso-octane

Results of iso-octane oxidation are shown in Fig. 3, where the molar fractions of fuel, CO and CO_2 are shown as a function of the reactor length. The temperature profile of the reactor is also reported together with that of the non-reacting case. The initial temperature drop is due to an unheated section at the reactor entrance [53], rather than endothermic reactions. Iso-octane starts to react at approximately 200 mm, whereas CO formation is not detectable until 400 mm, indicating significant chemistry prior to CO detection. CO_2 starts to be detected since 600 mm and its formation is companied by evident temperature increase relative to the non-reacting case. These results were modelled using the recent iso-octane models from Atef et al. [12] and two gasoline surrogate models from Mehl et al. [10] and Andrae [62], as shown in Fig. 3. Among these models, the Mehl model best reproduces the measured species profiles, although the CO_2 is over-predicted at the last stage of the reaction. The Atef model over-predicts the consumption of iso-octane, but best captures the formation of CO and CO_2. The Andrae model [62], on other hand, under-predicts the oxidation rate of iso-octane as evidenced by the results of all three species.

Results of intermediate species in the oxidation of iso-octane are reported in Fig. 4. Except for the unanalysed formaldehyde, the detected intermediates are consistent with those previously reported in flow reactors [64, 65], JSR [66], and RCM [67].

Major reaction pathways leading to the formation of C_7 olefins and isobutylene (IC4H8) are shown in Fig. 5. The four C_7 olefins, XC7H14 (2,4-dimethyl-1-pentene), YC7H14 (2,4-dimethyl-2-pentene), OC7H14 (4,4-dimethyl-2-pentene), and PC7H14 (4,4-dimethyl-1-pentene), along with isobutylene, are the primary products of iso-octane oxidation, and their formation can be explained by the β-scission of AC8H17, BC8H17, and DC8H17 radicals (Fig. 5). The relative abundance of the C_7 olefins follows the order of YC7H14≈OC7H14>XC7H14>PC7H14. This measured trend agrees well with the previous results in the Penn State flow reactor [65] obtained under a similar condition, 9 atm., 919 K, ϕ of 0.05, and a shorter residence time of 0.09 s. Nevertheless, none of the selected models reproduces the formation of these C_7 olefins adequately. The Andrae model [62] apparently best predicts the formation of all isomers up to 600 mm except YC7H14. However, the peak molar fractions of these olefins are all predicted later than

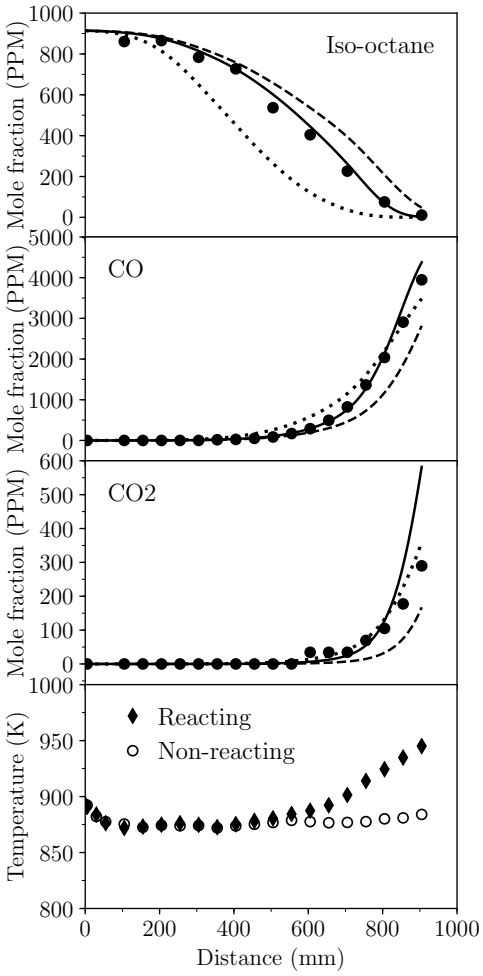

Figure 3: Evolution of iso-octane, CO, CO_2 in the oxidation of neat iso-octane, and the gas temperature of the reacting and non-reacting cases. Symbols are experiment results, curves are modelling results by Mehl et al. [10] (solid lines), Andrae [62] (dashed lines), and Atef et al. [12] (dotted lines).

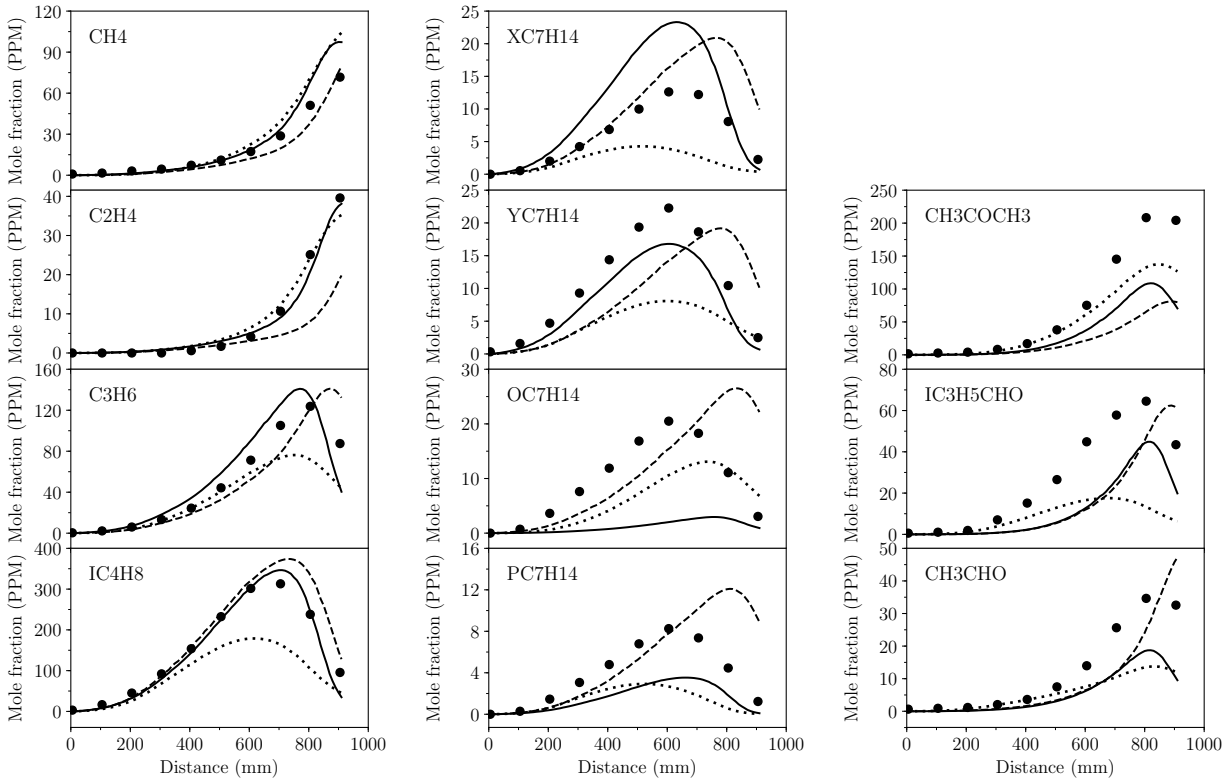

Figure 4: Evolution of intermediate species in the oxidation of neat iso-octane. Symbols are experiment results, curves are modelling results by Mehl et al. [10] (solid lines), Andrae [62] (dashed lines) and Atef et al. [12] (dotted lines) (Structures of C_7 olefins and oxygenated species are shown in Fig. 5 and ensuring discussion).

the experiment by this model. The Mehl model better captures the peak location, but overpredicts the formation of XC7H14 and underpredicts the other three. The Atef model [12], on the other hand, underpredicts the olefin formation in all cases. A further analysis is provided at the end of this section to understand the discrepancy between experiment and models in the formation of these primary products. Note that compared with smaller hydrocarbons discussed below, these C_7 species bear more fuel carbons than their molar fractions suggest, and when plotted on the same basis, e.g. C_1, the discrepancy between model and experiment will be amplified by a larger extent than those of smaller species. Therefore, major improvement is evidently needed for modelling the formation of these olefins.

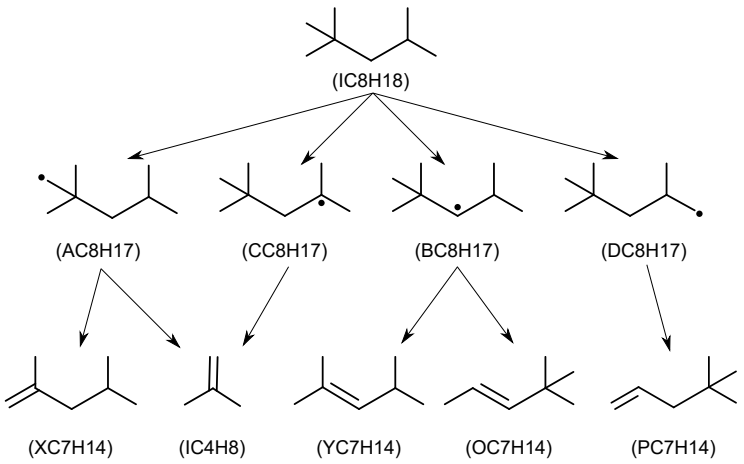

Figure 5: Reaction pathways of iso-octane for the formations of C_7 olefins and IC4H8.

Isobutylene (IC4H8) is the most abundant intermediate species detected at the condition. The formation pathway can be explained by the decompositions of AC8H17 and CC8H17 radicals, via β-scission occurring on the main carbon chain, as shown in Reactions 1 and 2. The profile of IC4H8 is well predicted by Mehl et al. [10], slightly over-predicted by Andrae [62], but significantly under-predicted by the latest model from Atef et al. [12].

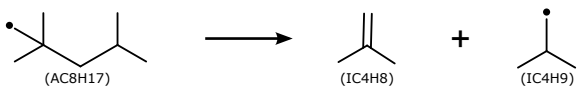

(1)

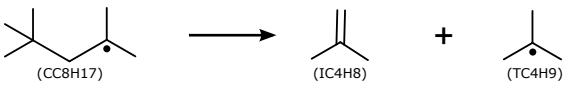

(2)

For oxygenated intermediates, acetone (CH3COCH3) is detected as the most abundant species. This was also

observed by Chen et al. [65] and they explained the production of acetone using the Waddington mechanism [68, 69], as shown in Reactions 3 to 5. The Waddington mechanism can also explain the formation of acetaldehyde (CH3CHO), another major oxygenate intermediate, by starting with propylene.

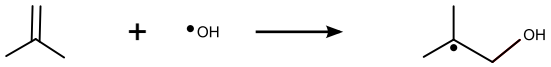

(3)

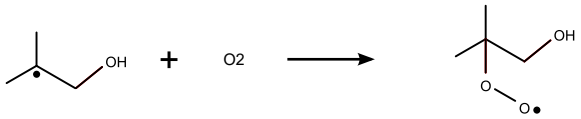

(4)

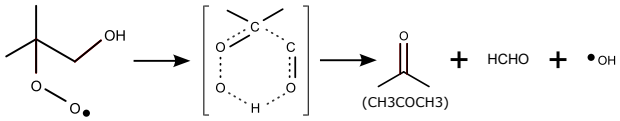

(5)

Methacrolein (IC3H5CHO) is detected as another major oxygenated intermediate. Its formation can be explained by Reactions 6 to 8 as proposed by Chen et al. [65], Curran et al. [8], and the recent AramcoMech 2.0 model [63]. Considering the lean conditions used in the experiments, methacrolein may also be formed by the IC4H7O radical reacting with oxygen molecule, as shown in Reaction 9. Modelling results show that the existing models all under-predict the molar fractions of these oxygenated compounds, but the Mehl model reasonably captures the positions where the peak value occurs.

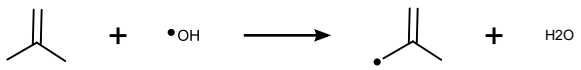

(6)

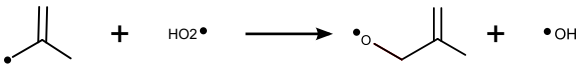

(7)

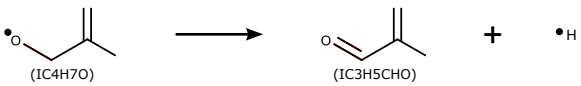

(8)

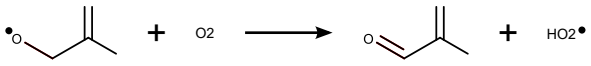

(9)

Smaller species, including methane (CH4), ethylene (C2H4), and propylene (C3H6), were also detected. Note that propylene forms earlier and in a larger quantity than ethylene, consistent with the oxidation of branched paraffins. The Mehl model again performs the best in reproducing the formation of these species, with the other two models also agreeing reasonably with the experiment.

Overall, among the models investigated, the gasoline surrogate model from Mehl et al. [10] best reproduces the species profiles from the oxidation of iso-octane at 900 K and 10 bar in the flow reactor, particularly for major species including fuel, CO, and isobutylene. The modelling for C_7 olefins and oxygenated intermediates nevertheless needs improvement.

It is noted that the iso-octane models used in this work all originate from the Curran model [8] which reasonably reproduced the formation of C_7 olefins in the Penn State flow reactor available at the time. A comparison between the Mehl model and the Curran model in simulating flow reactor data from Penn State and this work is shown in Fig. 6, with the Curran model performing consistently better for all C_7 olefins except YC7H14. Despite this difference, both models reproduce the formation of iso-butylene closely. The Andrae model (as shown in Fig. 4) has very similar performance to the Curran model in these cases.

Reaction flux analysis is then conducted at 200 mm in our reactor (corresponding to ~5% of fuel consumption), with results are shown in Fig. 7. The two models vary in many aspects, including the formation of iso-octyl radicals (C8H17), subsequent reactions of ROO radicals, and formation of C_7 and C_4 olefins. The largest discrepancy between the two models is in the formation of OC7H14, for which the Mehl model substantially under-predicts the measurement, whereas the Curran model agrees very well with both sets of data. This can be explained by the fact that only 1.3% of BC8H17 radicals are converted to OC7H14, which is an order of magnitude lower than that in the Curran model, although the Mehl model predicts 20% more BC8H17 radical. The difference in other C_7 olefins formed can also be explained in a similar manner.

This analysis demonstrates why both models reproduce the formation of iso-butylene similarly well. Iso-butylene is primarily produced from the β-scission of AC8H17 and CC8H17 radicals. The two channels, respectively, convert

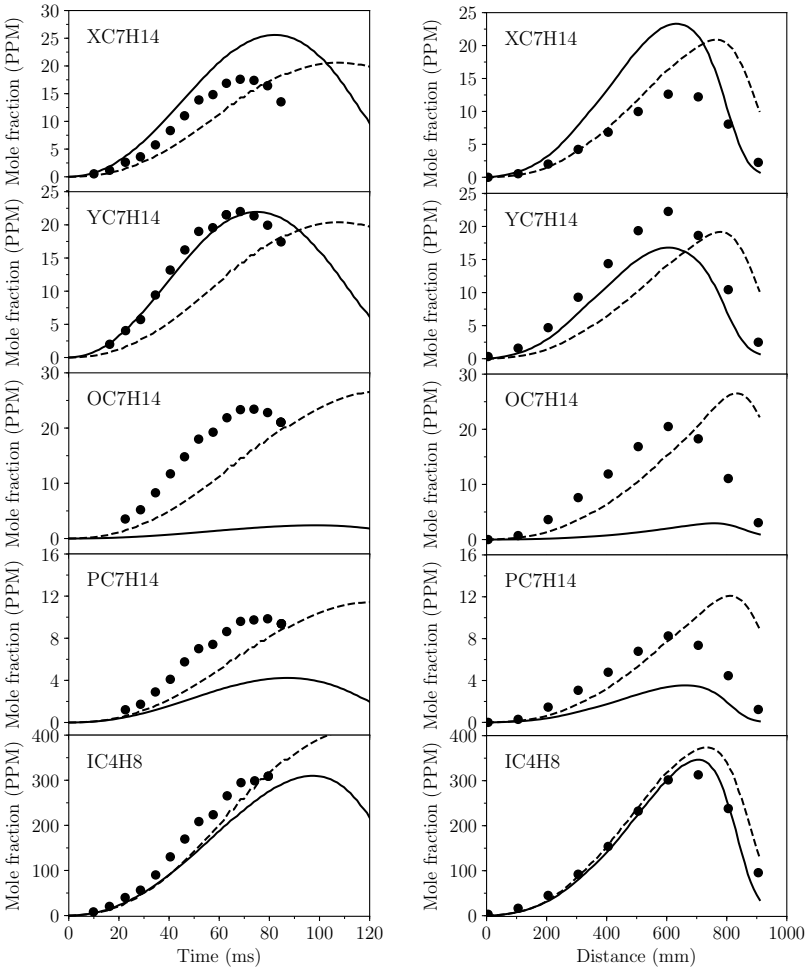

Figure 6: Modelling of C_7 and C_4 olefins in iso-octane oxidation using the Mehl model (solid line) and the Curran model (dashed line). (a) flow reactor data from Penn State at 9 atm., 919 K, equivalence ratio of 0.05, and total residence time of 0.09 s. (b) flow reactor data from this work at 10 atm., 900 K, equivalence ratio of 0.058, and total residence time of 0.27 s.

16.4% and 22.3% of the fuel carbon to iso-butylene as predicted by the Mehl model, and 29.1% and 7.2% by the Curran model. The total fuel carbon converted to the C_4 olefin, therefore, is 38.7% and 36.3%, respectively, which indicates good agreement between the two models despite the very different contributions from individual channels.

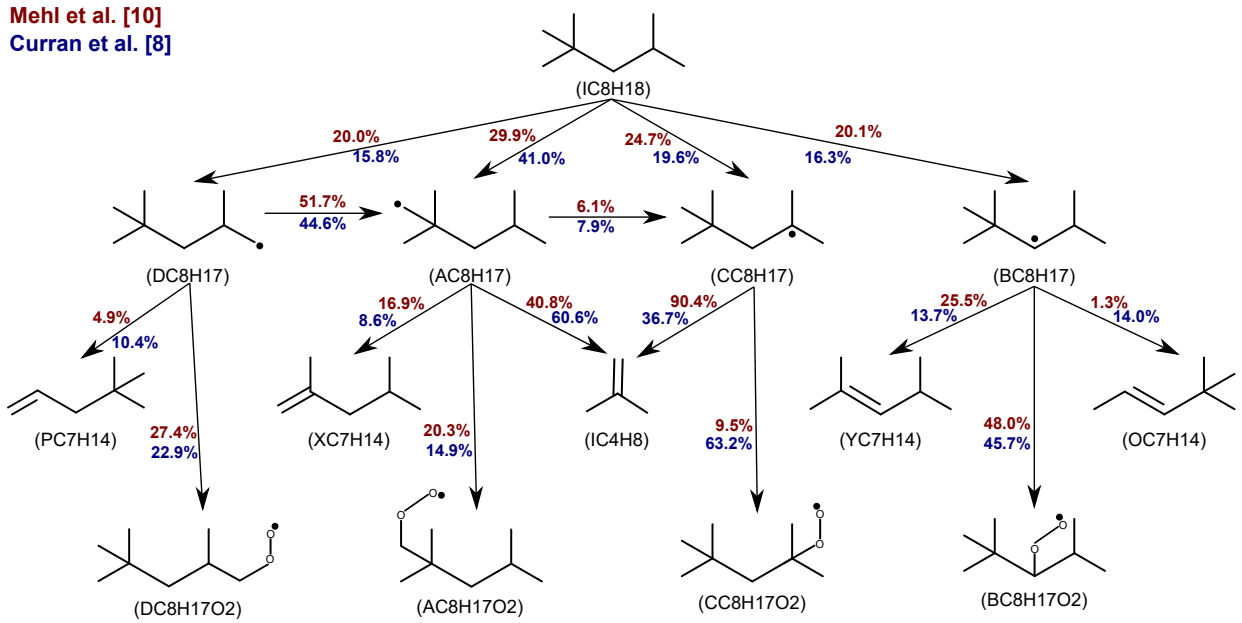

Figure 7: Reaction flux of iso-octyl radicals (C8H17) and subsequent reactions in the oxidation of iso-octane at 200 mm of the reactor. Analysis on data reported in this work at 10 bar, 900 K, and equivalence ratio of 0.058.

3.1.2. Ethanol

Results of ethanol oxidation are shown in Fig. 8, where the molar fractions of fuel, CO and CO_2 are shown as a function of the reactor length. Compared with iso-octane, ethanol is more reactive at the condition, as indicated by the faster consumption of ethanol and more significant CO to CO_2 conversion near the end of the reactor. The four selected models perform similarly well in simulating the oxidation of ethanol in that the profiles of ethanol and CO are accurately reproduced up to 500 mm. However, more significant discrepancies are observed near the end of the reactor, where the opposite trend in modelling CO (underpredicted) and CO_2 (overpredicted) suggests that the kinetics of CO to CO_2 conversion is too fast in all the models. This could be due to the CO oxidation chemistry having not been validated in the ultra-lean conditions used here. Similar discrepancy has been observed with other fuels when CO converts to CO_2 at significant rates, indicating that this is not a problem specific to ethanol.

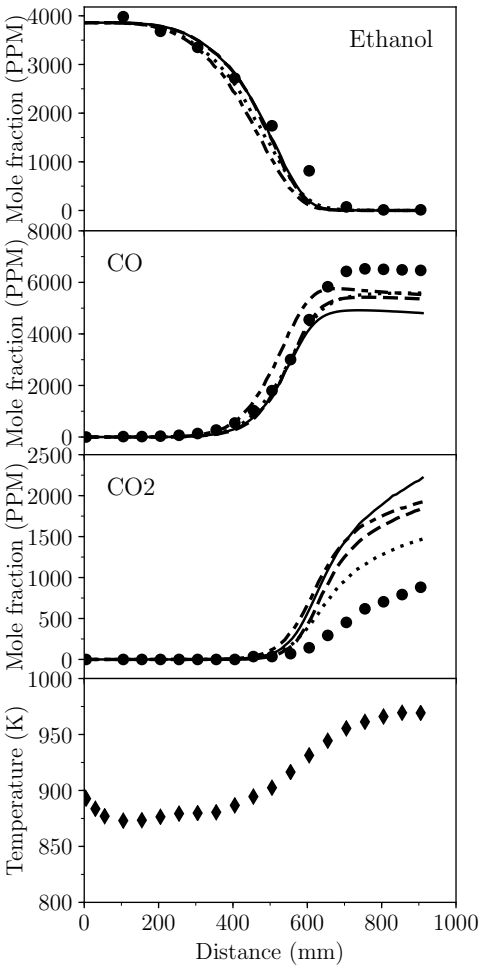

Figure 8: Evolution of ethanol, CO, and CO_2 from neat ethanol oxidation, and the gas temperature along the reactor. Symbols are experiment results, curves are modelling results by Mehl et al. [10] (solid lines), Mittal et al. [29] (dotted lines), AramcoMech 2.0 [63] (dashdot lines), and Andrae [62] (dashed lines).

Sensitivity analysis for the CO formation is conducted at 600 mm using the Mehl model (Fig. 9). The sensitivity coefficient is defined as follows:

$$SC = \frac{CO_i - CO_{ref}}{CO_{ref}}$$

where CO_i denotes the CO formation by doubling the A-factor of the i^{th} reaction, and CO_{ref} represents the CO formation with the original A-factor. Not surprisingly, the most sensitive reaction is CO + OH = CO2 + H which is known for its predominant role in CO oxidation. However, the absolute impact of this reaction is small, as indicated by the sensitivity coefficient. Examination of the Arrhenius parameters of this reaction, in fact, finds that the four models give very similar rate constants at 600 mm where the local temperature is 930 K, which is $1.57 \times 10^{11} \mathrm{cm}^3/\mathrm{mol/s}$ by Mittal et al. [29] and AramcoMech [63], $1.70 \times 10^{11} \mathrm{cm}^3/\mathrm{mol/s}$ by Mehl et al. [10], and $1.78 \times 10^{11} \mathrm{cm}^3/\mathrm{mol/s}$ by Andrae [62]. These k values also agree closely with the theoretical calculation by Joshi and Wang, $1.53 \times 10^{11} \mathrm{cm}^3/\mathrm{mol/s}$ [70]. Therefore, the uncertainty of the rate constant of this reaction should not be the cause of the observed discrepancy in CO and CO_2. Alternatively, the OH concentrations vary considerably among the models, as shown in Fig. 10 as a function of the reactor length. The highest OH concentration from the Mehl model explains why this model predicts the fastest CO to CO_2 conversion in Fig. 8. In comparison with the experiment, it is possible that all models overpredict the OH concentration under the ultra-learn condition, therefore result in the overly fast CO conversion. Further investigation is required to fully clarify this issue.

Results of major intermediate species from ethanol oxidation are shown in Fig. 11, including acetaldehyde, ethylene, and methane. Consistent with other experimental studies [23, 30, 71], the most abundant intermediate species of ethanol oxidation is acetaldehyde. According to the gasoline surrogate model of Mehl et al. [10], acetaldehyde is produced mainly from Reaction 10.

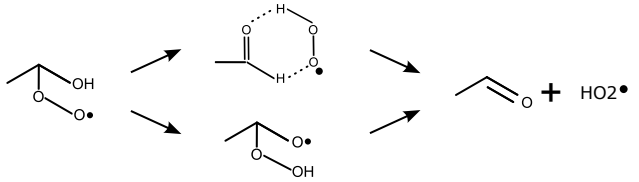

(10)

The profile of acetaldehyde is overall well reproduced by the Mehl model, as is the methane profile. However,

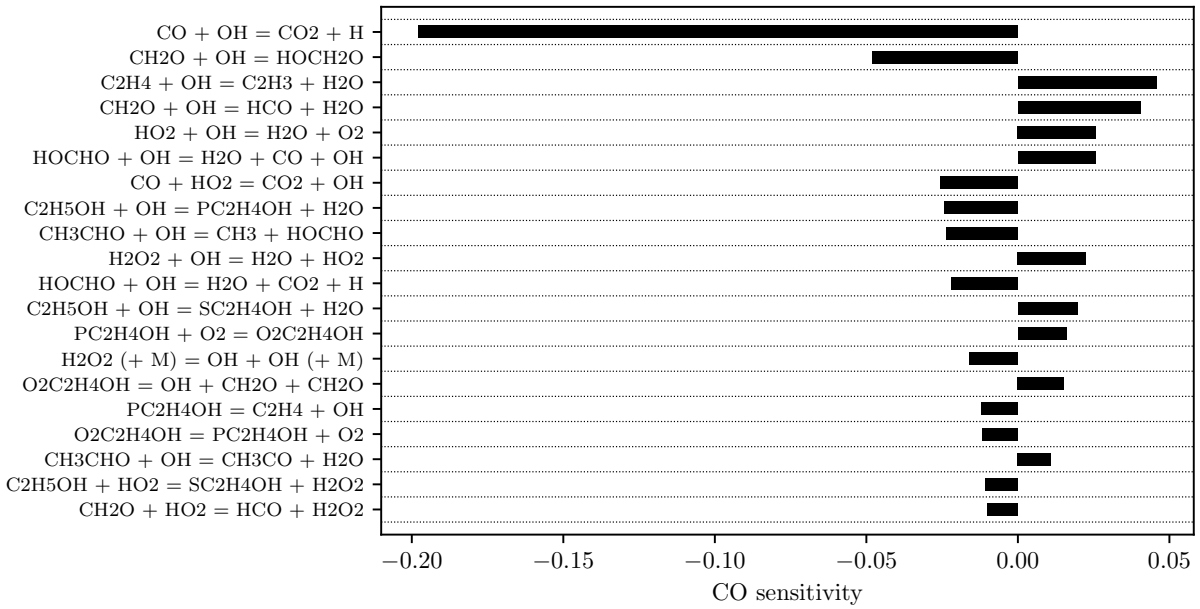

Figure 9: Brute force sensitivity analysis of CO formation at 600 mm in the oxidation of ethanol at 900 K and 10 bar.

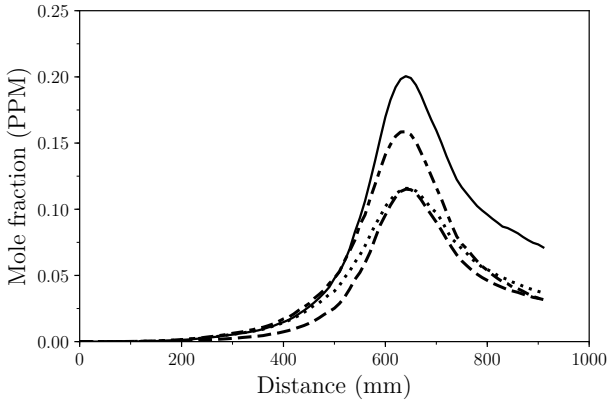

Figure 10: Evolution of OH radical from neat ethanol oxidation. Modelling results by Mehl et al. [10] (solid lines), Mittal et al. [29] (dotted lines), AramcoMech 2.0 [63] (dashdot lines), and Andrae [62] (dashed lines).

this model greatly over-predicts ethylene concentrations. In comparison, the predictions from the Andrae model [62] match the ethylene profile well but not the other species. The model from Mittal et al. [29] over-predicts all three species, while AramcoMech 2.0 [63] over-predicts methane and acetaldehyde but under-estimates ethylene. Overall, these models demonstrate little consistency among themselves in simulating the intermediate species, which is in contrast to the situation in modelling CO and CO_2. This suggests that the discrepancy in modelling intermediate species does not cause the later issue in modelling CO oxidation, further supporting that the latter is not an issue specific to ethanol chemistry.

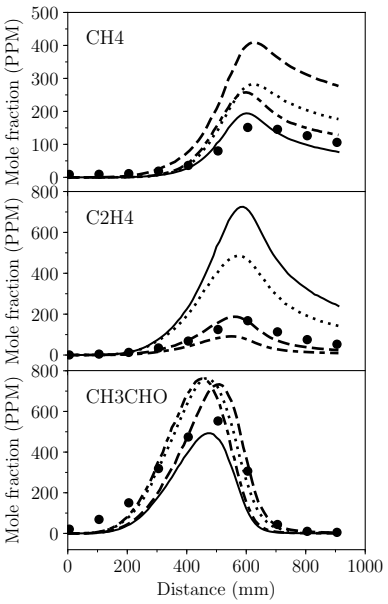

Figure 11: Evolution of intermediate species in the oxidation of neat ethanol. Symbols are experiment results, curves are modelling results by Mehl et al. [10] (solid lines), Mittal et al. [29] (dotted lines), AramcoMech 2.0 [63] (dashdot lines) and Andrae [62] (dashed lines).

3.1.3. Toluene

Compared with iso-octane and ethanol, toluene has much lower reactivity and barely reacts at 900 K. Therefore, experiment for toluene is conducted at a higher temperature, 930 K. Even at this temperature, CO formation is substantially lower than that of iso-octane and ethanol, as shown in Fig. 12. The six models used for simulating the oxidation of toluene show considerably different performance. The models of Metcalfe et al. [15] and Zhang et al. [19] produce the closest agreement with the measured toluene and CO profiles. Note that the Zhang model is developed from the

Metcalfe model. The other four models, Mehl et al. [10], Yuan et al. [16], Andrae [62], and Pelucchi et al. [21], all over-predict the reactivity of toluene to various extents. Due to the low reactivity, the only intermediate species detected is benzene, which is over-predicted by models from Andrae [62] and Pelucchi et al. [21], but under-predicted by the others. Benzaldehdye is another important intermediate species in the oxidation of toluene [15, 16] but is not analysed here due to its retention time overlapping with toluene.

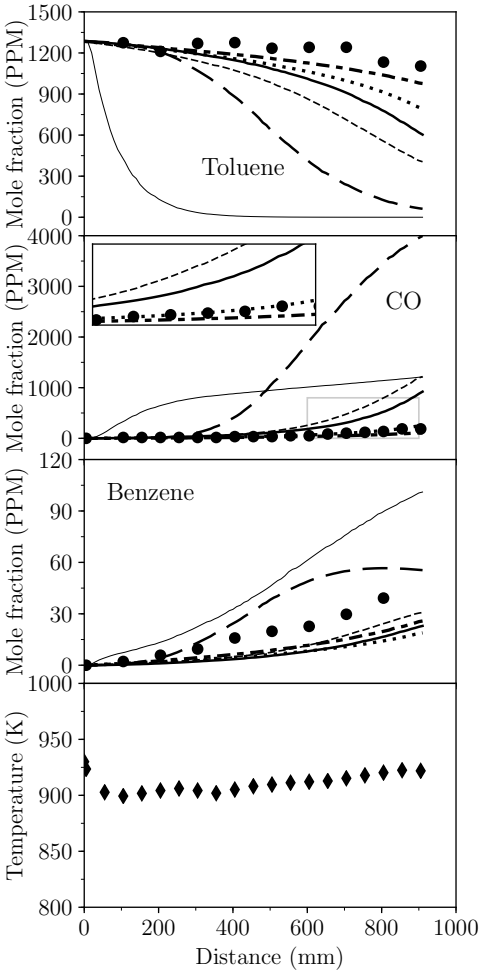

Figure 12: Evolution of toluene, CO, benzene in the oxidation of neat toluene, and the gas temperature along the reactor. Symbols are experiment results, curves are modelling results by Metcalfe et al. [15] (dashdot lines), Zhang et al. [19] (dotted lines), Mehl et al. [10] (solid lines), Yuan et al. [16] (thin dashed lines), Pelucchi et al. [21] (large dashed lines), and Andrae [62] (thin solid lines).

For the two best performing models from Metcalfe et al. [15] and Zhang et al. [19], it is noted that neither has been incorporated in a gasoline surrogate model. This makes them unavailable to the subsequent investigation of toluene-

containing mixtures in this work. An attempt is therefore made to improve the gasoline surrogate model of Mehl et al. [10] which has effectively reproduced the oxidation of iso-octane and ethanol. The exercise starts with sensitivity analysis on the CO formation in the oxidation of toluene at 930 K and 10 bar. The top 20 most sensitive reactions are shown in Fig. 13 for the reaction at 900 mm of the reactor. Notably, most of these reactions involve toluene or toluene-like species, and their sensitivity coefficients are of significant absolute value, indicating that variation of these rate constants will produce large impacts on the reactivity of toluene.

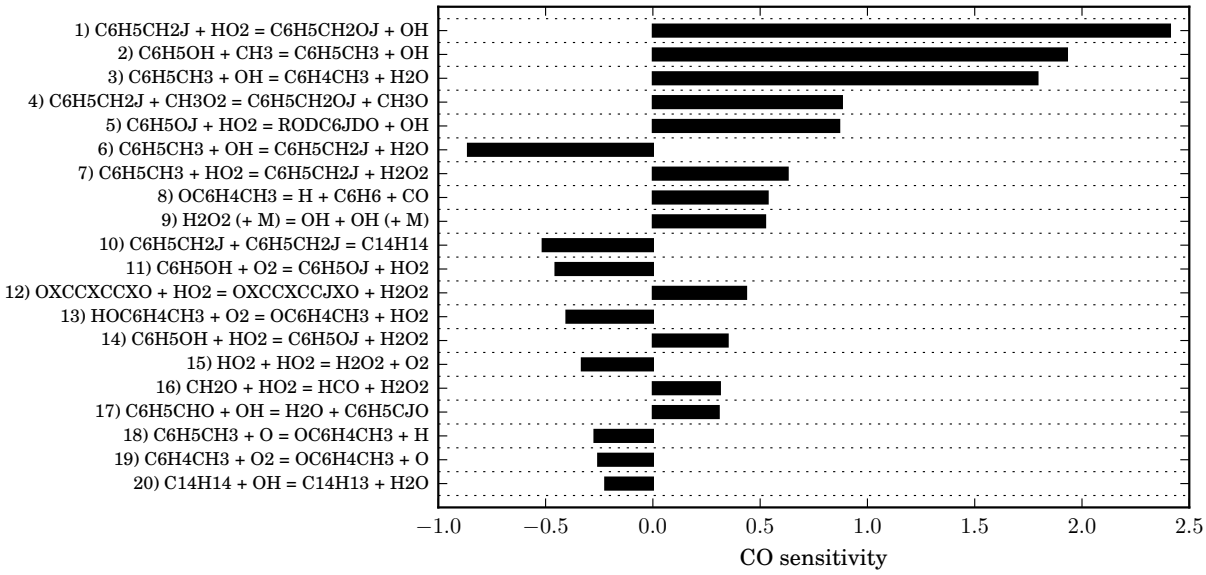

Figure 13: Brute force sensitivity analysis of CO at 900 mm for the toluene oxidation under 930 K and 10 bar using Mehl et al's gasoline surrogate model [10].

The top 10 most sensitive reactions are then examined to identify possible causes for the over-predicted CO in modelling the oxidation of toluene. In doing so, Arrhenius parameters of these reactions are compared with those in the latest literature, and when this is unavailable, with those in the Metcalfe model [15] which is based on a comprehensive review of toluene chemistry and apparently better predicts the CO formation.

For the most sensitive reaction in Fig. 13, benzyl radical + HO2, both models of Mehl et al. [10] and Metcalfe et al. [15] only specified the pre-exponential factor and assigned a zero value to the activation energy and temperature dependence factor. A recent theoretical calculation by da Silva and Bozzelli [72] found that this reaction is not barrierless at atmospheric pressure. This calculation, which was extended to high pressures by Zhang et al. [19], is

adopted in this work. In addition, the Arrhenius parameters of the 5th and 7th reactions are found to be different from that in the Metcalfe model [15] and therefore the values in the latter are used. The parameters of the 7th reaction is in fact originally from the comprehensive dataset of Baulch et al. [73].

For the other seven reactions, the original Arrhenius parameters from Mehl et al. [10] are used. This is because these parameters are either very similar to that in the Metcalfe model [15] (the 3rd, 6th, and 8th reactions) or do not appear in the Metcalfe model [15] (the 2nd and 4th reactions). Besides, the 9th reaction doesnt involve toluene, and the 10th reaction is not changed due to the much smaller impact relative to the others.

The three changes made to the toluene sub-model in the Mehl model are summarised in Table 3. The revised model is called 'adjusted Mehl model'. Comparison of the original and adjusted models is shown in Fig. 14, where significant improvement is observed in reproducing the CO and toluene profiles, indicating that the changes in Table 3 are useful.

It should nonetheless be emphasised that the adjusted model represents only a preliminary effort to improve the toluene model. It demonstrates that reasonable adjustments of selected reaction rates can significantly improve the simulation of neat toluene, which serves the purpose of targeting a model applicable to toluene-containing mixtures. Nevertheless, the adjustment is adhoc in nature and the model is not optimised for the proposed changes. Further development is undoubtedly needed. One obvious option is to substitute the toluene sub-model in the gasoline surrogate model with one of the best performing toluene models of Metcalfe et al. [15] or Zhang et al. [19]. However, simple substitution of the toluene sub-model is found to be no better than the adjusted model reported here, as shown in the Supplementary Information. Dedicated model optimisation is therefore called for in future research.

Table 3: Changes to Mehl model [10] (adjusted values in bold, units in cm^3-mol-sec-cal).

Top sensitivity reactions	**A**	**n**	**E_A**	Reference
1) 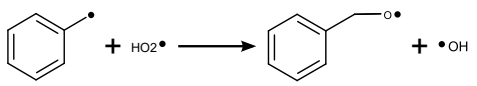	(5e12) **1.12e24**	(0.00) **-2.93**	(0.00) **12339**	[19][a]
5) 	(5e12) **2.00e12**	(0.00) **0.00**	(0.00) **0.00**	[15]
7) 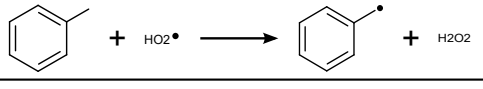	(7.00e02) **3.97e11**	(3.00) **0.00**	(12000) **14069**	[73]

[a] This rate constant from Zhang et al. [19] is at 10 bar

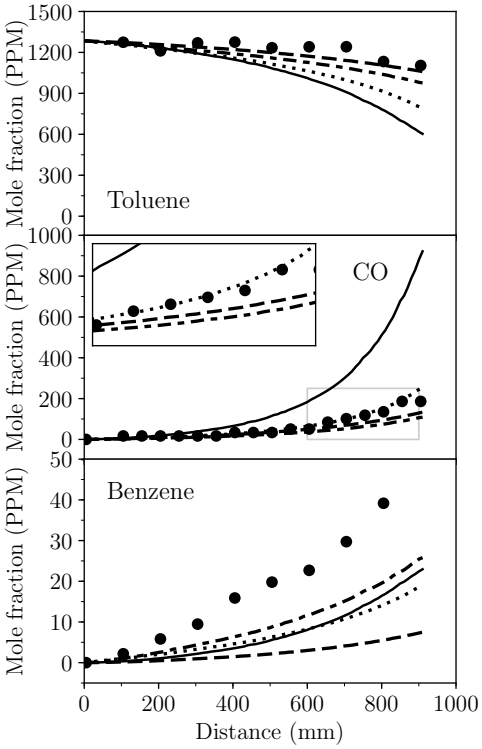

Figure 14: Evolution of species from the toluene oxidation at 930 K and 10 bar, and the modelling results by Metcalfe et al. [15] (dashdot lines), Zhang et al. [19] (dotted lines), Mehl et al. [10] (solid lines), and adjusted Mehl model (dashed lines).

3.2. Binary mixtures

Binary mixtures of ethanol/iso-octane, toluene/iso-octane, and ethanol/toluene are studied at various blending ratios. Only the CO data are measured for these mixtures, which are simulated using the gasoline surrogate model from Mehl et al. [10]. The adjusted Mehl model performs identically to the original model in the absence of toluene; therefore, it is only used to simulate toluene-containing mixtures. The same applies to the following sections for gasoline reference fuels and their mixtures with ethanol.

3.2.1. Ethanol and iso-octane mixtures

The CO profiles of three ethanol/iso-octane mixtures containing 0.239, 0.414, and 0.739 mole fraction of ethanol are shown in Fig. 15, together with the two neat fuels. Ethanol is clearly more reactive than iso-octane at this test condition, and the reactivity of the mixture increases with higher ethanol content. Kinetic modelling results are shown

in Fig. 16, where the Mehl model reproduce the CO formation very well and suggest that the potential interactions between iso-octane and ethanol are well captured by the models at this condition.

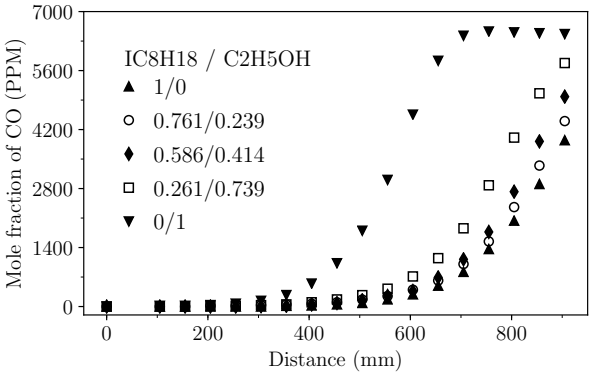

Figure 15: Measured CO profiles of iso-octane/ethanol mixtures (blended by mole fraction).

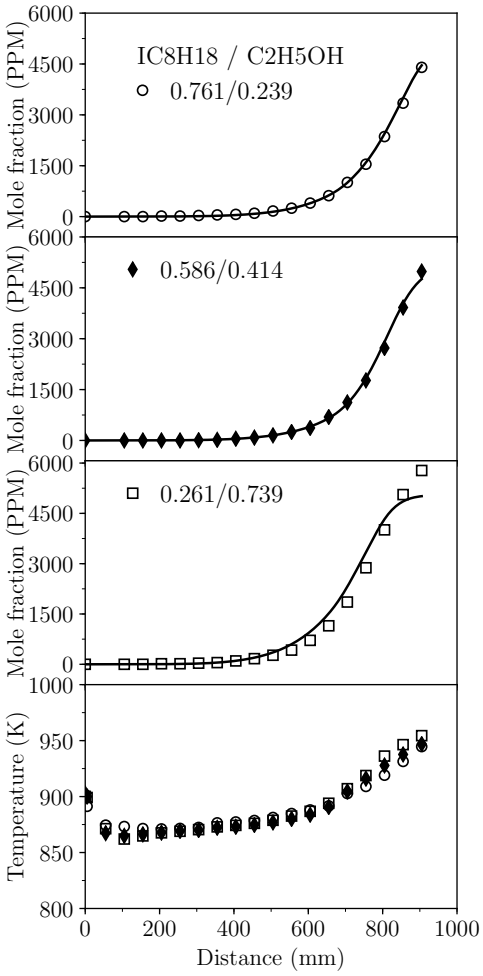

Figure 16: Evolution of CO and gas temperature in the oxidation of iso-octane/ethanol mixtures (blended by mole fraction) at 900 K and 10 bar. Symbols are experiment results, curves are modelling results by the original Mehl model [10].

3.2.2. Toluene and iso-octane mixtures

The CO profiles of three toluene/iso-octane mixtures (0.25, 0.50, and 0.75 mole fraction of toluene) are shown in Fig. 17, together with the two neat fuels. Since iso-octane is more reactive than toluene, the reactivity of the mixture increases with higher iso-octane content.

Results of kinetic modelling are shown in Fig. 18. Given the original Mehl model [10] significantly over-predicted the oxidation of neat toluene (Fig. 12), the model is expected to have difficulty in reproducing toluene-containing mixtures. Indeed, Fig. 18 shows that the discrepancy between the measurement and model (solid line) increases from 352% to 512% and to 793% as the mole fraction of toluene increases from 0.25 to 0.5 and to 0.75, consistent with the problematic toluene model playing a progressively greater role.

In contrast, the adjusted model (dashed line) performs better for these mixtures, and consistent with the improved toluene sub-model, the model performs better at higher toluene contents. However, this model (identical to the original model without toluene) also well reproduces the oxidation of neat iso-octane (Fig. 3). It is therefore unexpected that the performance of the model deteriorates with more iso-octane in the mixture. From the experiment, it is noted that the addition of the first 0.25 mole fraction of toluene suppresses the CO formation much more than each subsequent addition, indicating some non-linear kinetic interactions between the two compounds during oxidation. The discrepancy between the experiment and model suggests that such interactions are not adequately simulated, although it could also be due to the adjusted model having not been fully validated for the oxidation of neat toluene.

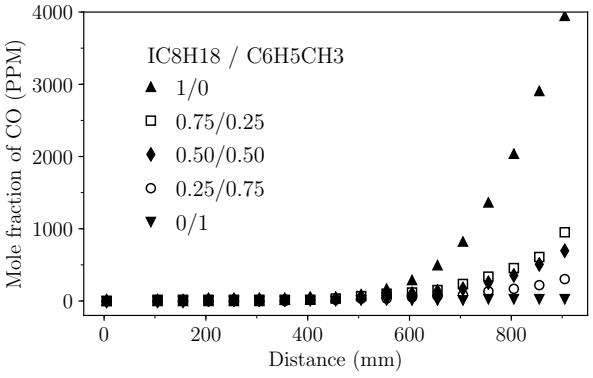

Figure 17: Measured CO profiles of iso-octane/toluene mixtures (blended by mole fraction).

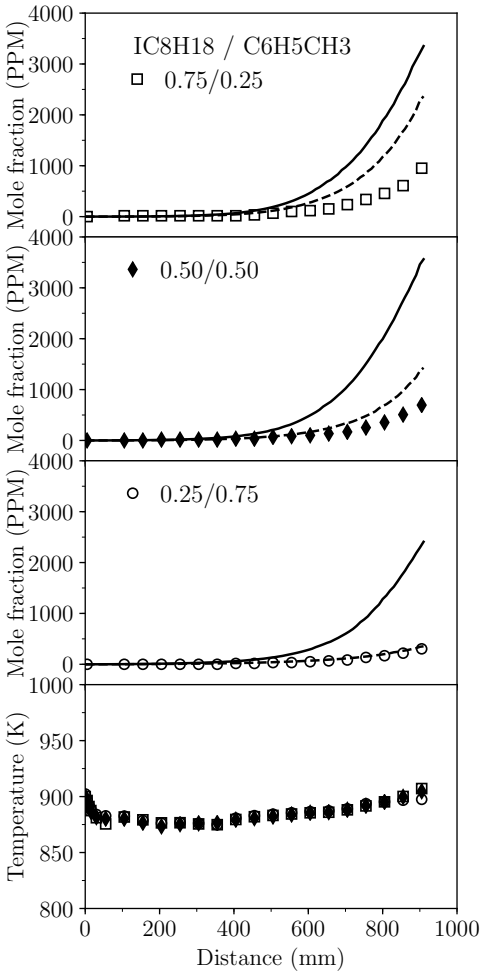

Figure 18: Evolution of CO and gas temperature in the oxidation of iso-octane/toluene mixtures (blended by mole fraction) at 900 K and 10 bar. Symbols are experiment results, curves are modelling results by the original Mehl model [10] (solid lines) and the adjusted model (dashed lines).

3.2.3. Ethanol and toluene mixtures

The CO profiles of three ethanol/toluene mixtures (0.25, 0.50, and 0.75 molar fraction of toluene) are shown in Fig. 19, together with the two neat fuels. Since ethanol is much more reactive than toluene, the reactivity of the mixture increases with higher ethanol content. Kinetic modelling results are shown in Fig. 19. Similar to the results in Fig. 18, the adjusted Mehl model performs better than the original model due to the improved toluene chemistry. It is noted that the original and adjusted models differ only by the three reactions in Table 3 that involve toluene-related species and HO2 radicals. The fact that the adjusted model effectively reproduces the CO formation of the ethanol/toluene mixtures, while the original model does not, suggests that HO2 is the key species to the interaction of toluene and ethanol, and cross reactions between fuel-like species from toluene and ethanol are not important at the condition.

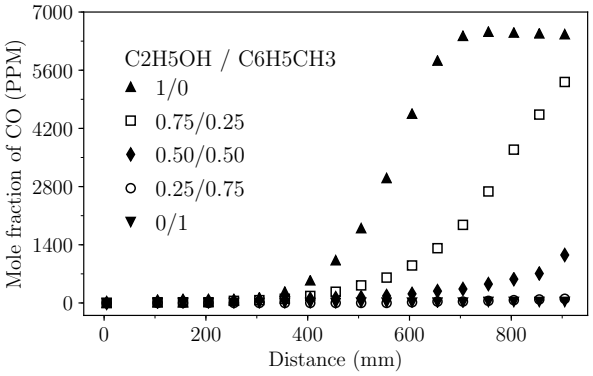

Figure 19: Measured CO profiles of ethanol/toluene mixtures (blended by mole fraction).

Results of the three pairs of binary mixtures, therefore, indicate that the existing chemical models are capable of simulating the oxidation for ethanol/iso-octane mixtures and to a large extent for ethanol/toluene mixtures, but they are unable to reproduce iso-octane/toluene mixtures, even though the adjusted Mehl model can effectively reproduce the oxidation of both neat toluene and neat iso-octane. Further model development on toluene is of obvious importance given the role of aromatics in practical fuels and in developing surrogate fuels to model practical fuels.

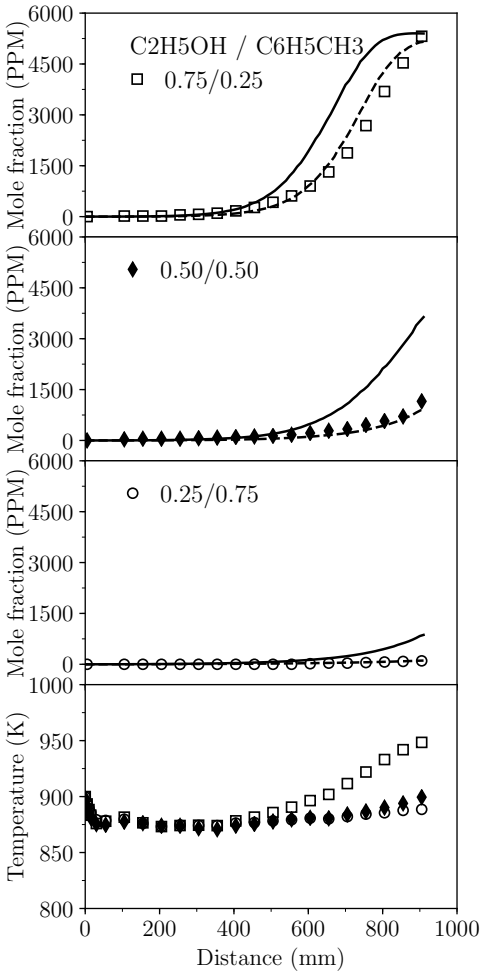

Figure 20: Evolution of CO and gas temperature in the oxidation of ethanol/toluene mixtures (blended by mole fraction) at 900 K and 10 bar. Symbols are experiment results, curves are modelling results by the original Mehl model [10] (solid lines) and the adjusted model (dashed lines).

3.3. Gasoline reference fuels

Two gasoline reference fuels with RON of 91 are studied, including a binary mixture PRF91 (iso-octane/n-heptane = 0.90/0.10 by mole, and a ternary mixture TRF91 (iso-octane/n-heptane/toluene = 0.449/0.162/0.390 by mole).

3.3.1. PRF91

Figure 21 shows the formation of CO and CO_2 and the consumption of fuel components in the oxidation of PRF91 as a function of the reaction length. The simulation results show that the Mehl model [10] well reproduces the profiles of CO, CO_2, and the two fuel components.

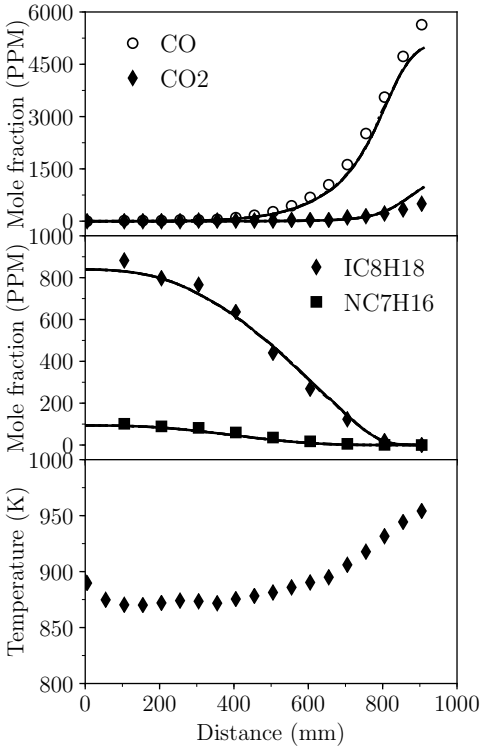

Figure 21: Evolution of iso-octane, n-heptane, CO, CO_2 in the oxidation of PRF91, and the gas temperature along the reactor. Symbols are experiment results, curves are modelling results by the original Mehl model [10].

Results of the intermediate species are shown in Fig. 22. The major species measured are similar to those from the oxidation of iso-octane due to the large fraction of iso-octane in PRF91. Overall, the results of C_1-C_4 hydrocarbons are well reproduced by these models, particularly isobutylene which is the most abundant intermediates measured. Consistent with the case of neat iso-octane, modelling of C_7 olefins and oxygenated compounds needs improvement.

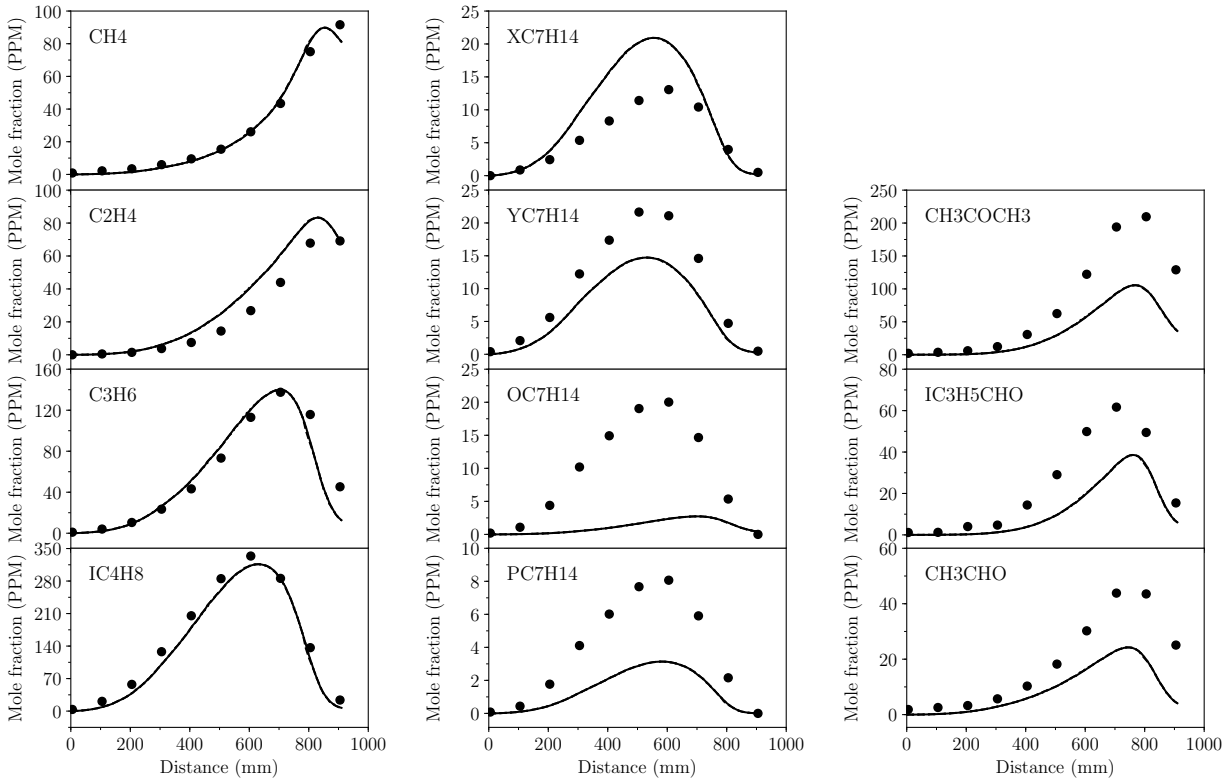

Figure 22: Evolution of intermediate species in the oxidation of PRF91. Symbols are experiment results, curves are modelling results by the original Mehl model [10].

3.3.2. TRF91-30

TRF91-30 is a simple gasoline surrogate with the research octane number of 91.3 differing from the motor octane number of (MON) of 86.1 [4], making it more relevant for practical gasoline (PRF91 has RON equal to MON; both 91 by definition). Figure 23 shows the formation of CO and CO_2 and the consumption of fuel components in the oxidation of TRF91-30 as a function of the reaction length. It is observed that the adjusted Mehl model performs better than the original model, but the discrepancy with measurement is still significant, e.g. for the consumption of toluene and n-heptane. Note that the consumption of toluene at 900 K here measured is significantly higher than that of neat toluene at 930 K (Fig. 12), indicating that toluene oxidation is enhanced in the presence of n-heptane and iso-octane. Both models predict such enhancement but to a much larger extent than the experiment, in consistent with the over-predicted CO formation in iso-octane/toluene mixtures in Fig. 18.

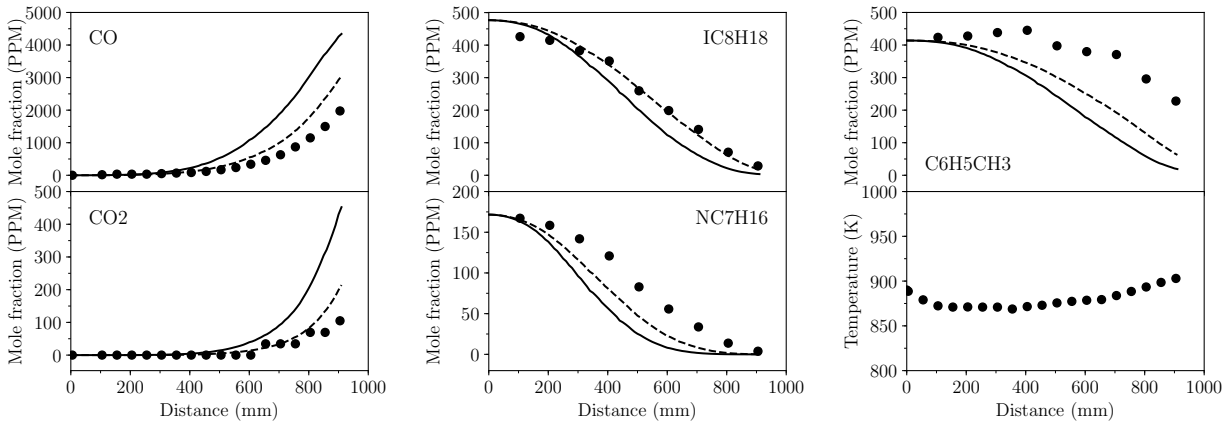

Figure 23: Evolution of iso-octane, n-heptane, toluene, CO, CO_2 in the oxidation of TRF91-30, and the gas temperature along the reactor. Symbols are experiment results, curves are modelling results by the original Mehl model [10] (solid lines) and the adjusted model (dashed lines).

The major intermediate species from the oxidation of TRF91-30 are shown in Fig. 24. With the presence of toluene, agreements between model and experiment are considerably poorer than in the case of PRF91 (Fig. 22), which is true for both models. Not only are the species molar fractions poorly predicted, but the location of the peaks all occurs earlier than the experiment (except for OC7H14), corresponding to the over-predicted consumption of fuel components in Fig. 23.

Investigation of the two gasoline reference fuels therefore demonstrated that the two models adequately reproduce

the oxidation of PRF91 but significantly over-predict the reactivity of TRF91-30, presumably due to the issue in the model of neat toluene. This finding is consistent with the results of binary mixtures in Section 3.2. Similar trend of results is reported by Javed et al. [45] who found that the Mehl model over-predicted the reactivity of fuel mixtures with high toluene contents in their RCM experiments at 10 bar below 900 K.

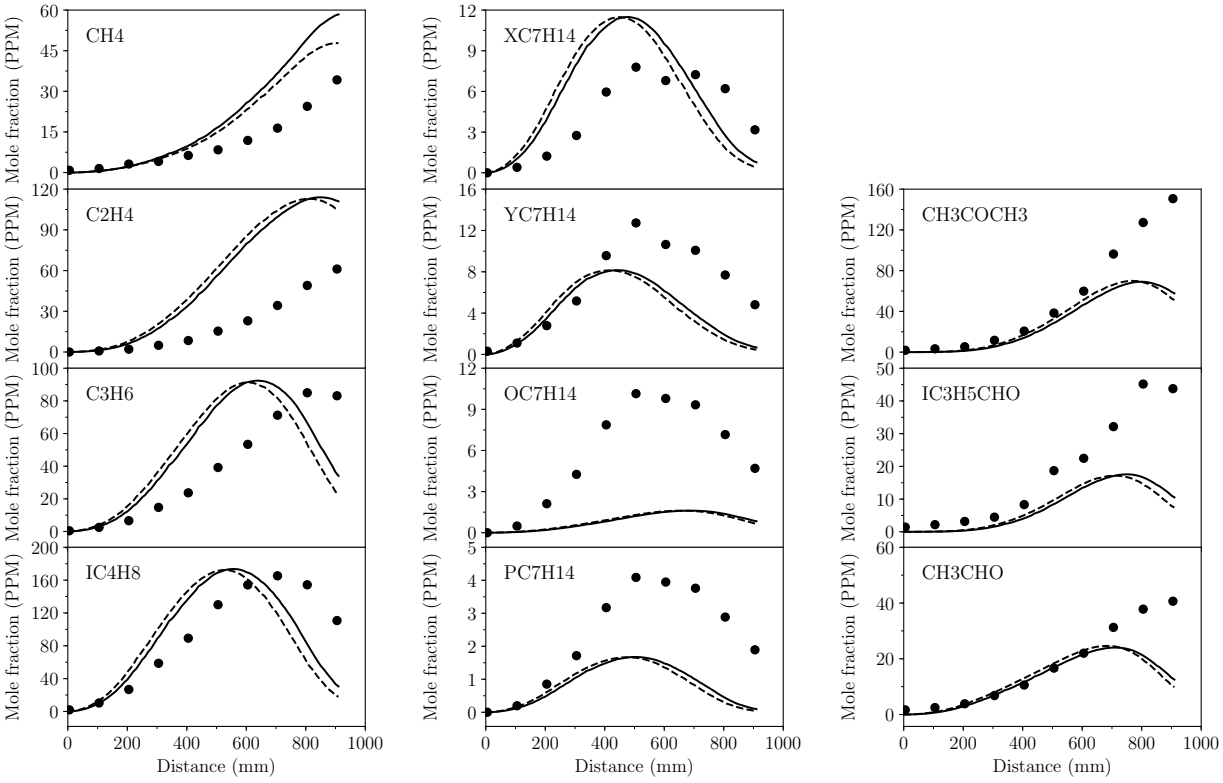

Figure 24: Evolution of intermediate species in the oxidation of TRF91-30 Symbols are experiment results, curves are modelling results by the original Mehl model [10] (solid lines) and the adjusted model (dashed lines).

3.4. PRF/ethanol and TRF/ethanol mixtures

3.4.1. PRF91 and ethanol mixture

A PRF91/ethanol mixture containing 0.737 mole fraction of ethanol (0.5 by volume) was studied. The measured profiles of CO, CO_2, and parent fuels are shown in Fig. 25 as a function of the reactor length, together with the modelling results. The Mehl model effectively reproduces the CO formation and the consumptions of the three fuel components, suggesting that the interactions among iso-octane, n-heptane, and ethanol are modelled adequately. It is

noted that near the end of the reactor, the model predicts lower CO/higher CO_2 molar fractions than the measurement. The discrepancy was also observed in the case of neat ethanol (Fig. 8) and again likely due to the chemistry related to CO to CO_2 conversion not validated at the ultra-lean condition.

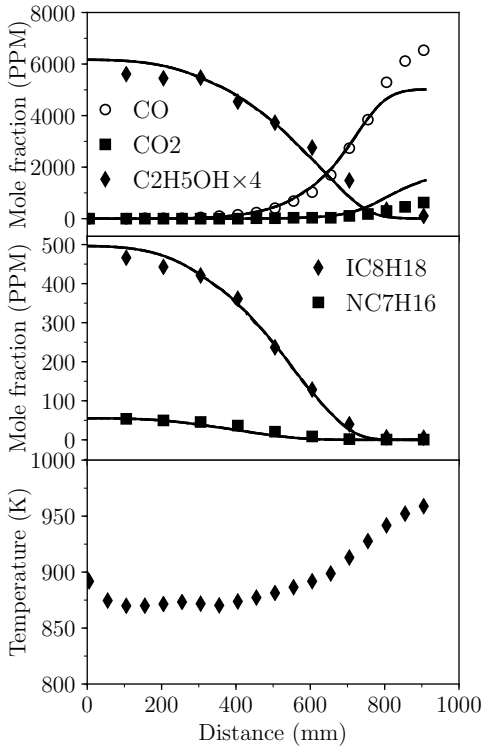

Figure 25: Evolution of iso-octane, n-heptane, ethanol, CO, CO_2 in the oxidation of PRF91 and ethanol mixture, and the gas temperature along the reactor. Symbols are experiment results, curves are modelling results by the original Mehl model [10].

With the large content of ethanol, acetaldehyde becomes the most abundant intermediate species whose profile is well reproduced by the model, as shown in Fig. 26. Note that acetaldehyde is a common product from the oxidation of both iso-octane and ethanol, which is effectively modelled for ethanol (Fig. 11) but not for iso-octane (Fig. 4). The well-matched acetaldehyde profile in Fig. 26 indicated that acetaldehyde is mostly formed from the oxidation of ethanol, the dominant component in the PRF91/ethanol mixture. For the same reason, most ethylene is also formed by ethanol; therefore, it is over-predicted by the model as in the case of neat ethanol (Fig. 11). Except for methane, all the other intermediates detected derive primarily from the oxidation of iso-octane, for which the modelling results are consistent with the case of neat iso-octane (Fig. 4).

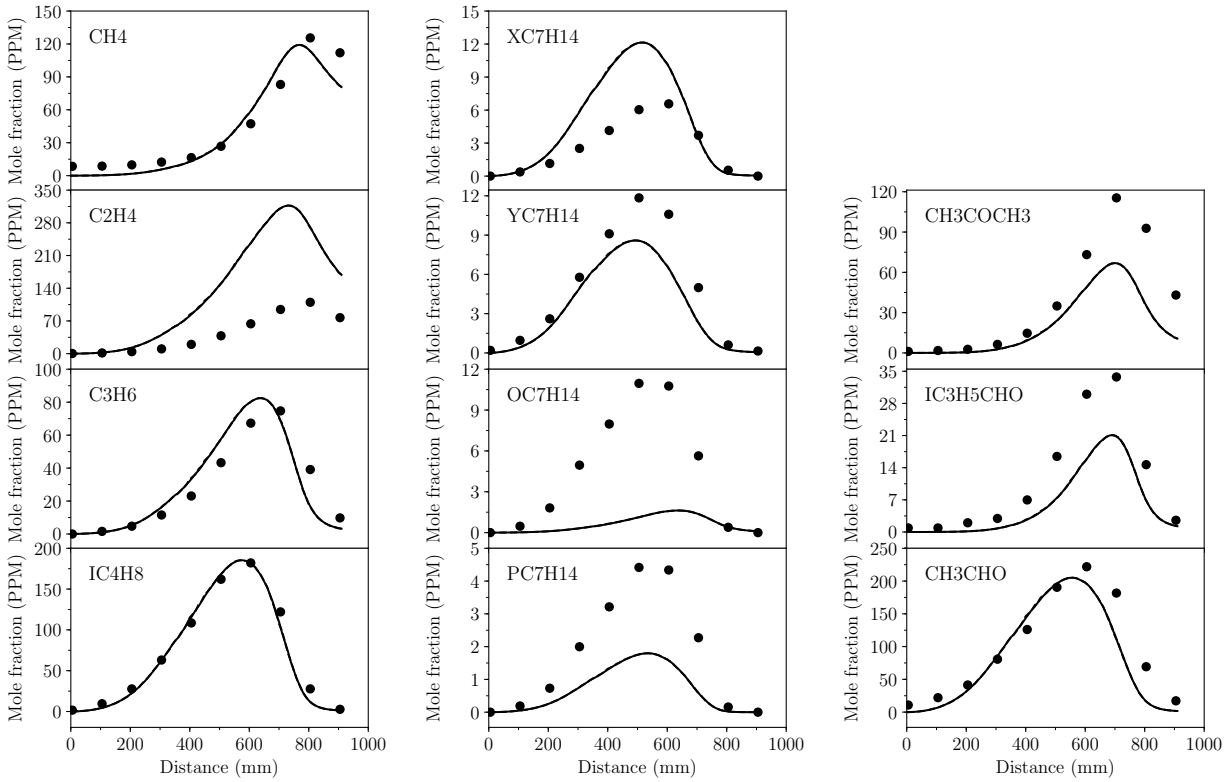

Figure 26: Evolution of intermediate species in the oxidation of PRF91 and ethanol mixture. Symbols are experiment results, curves are modelling results by the original Mehl model [10].

3.4.2. TRF91-30 and ethanol mixture

A mixture of TRF91-30 and ethanol containing 0.705 mole fraction of ethanol (0.5 by volume) is also tested. Results for CO, CO_2, and fuel components are shown in Fig. 27. Both the original and adjusted Mehl models reasonably reproduce the profiles of these species, presumably due to the small content of toluene in the mixture (0.115 mole fraction). For the same reason, the adjusted model performed only slightly better than the original model [10]. Nevertheless, noticeably larger discrepancy is observed than the case of PRF91/ethanol mixture (Fig. 25), still showing a possible impact of the problematic toluene model.

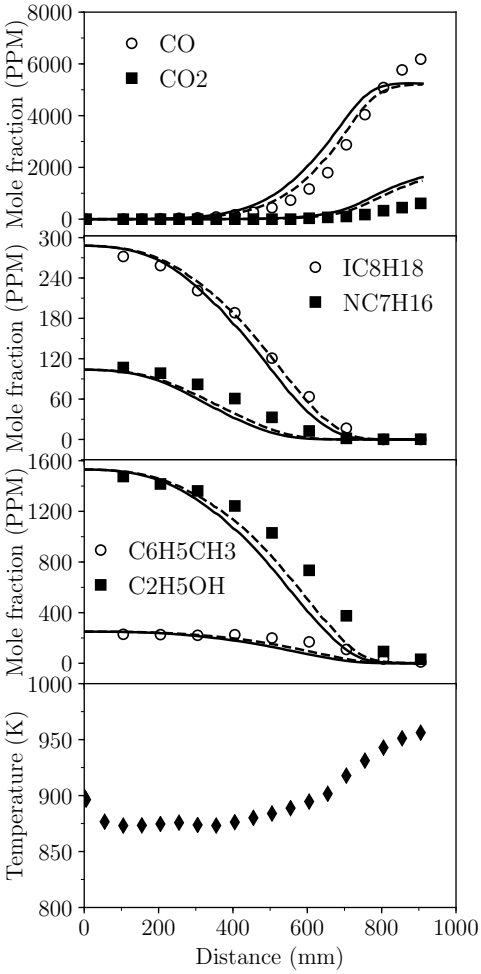

Figure 27: Evolution of iso-octane, n-heptane, toluene, ethanol, CO, CO2 in the oxidation of TRF91-30 and ethanol mixture, and the gas temperature along the reactor. Symbols are experiment results, curves are modelling results by the original Mehl model [10] (solid lines) and the adjusted model (dashed lines).

Profiles of intermediate species are shown in Fig. 28. Due to the high concentration of ethanol, the measured

results are similar to that of PRF91/ethanol mixture in Fig. 26. However, most peaks shift upstream relative to the experiment. This could be due to the over-predicted reactivity of toluene, as also observed in the case of TRF91-30 (Fig. 24).

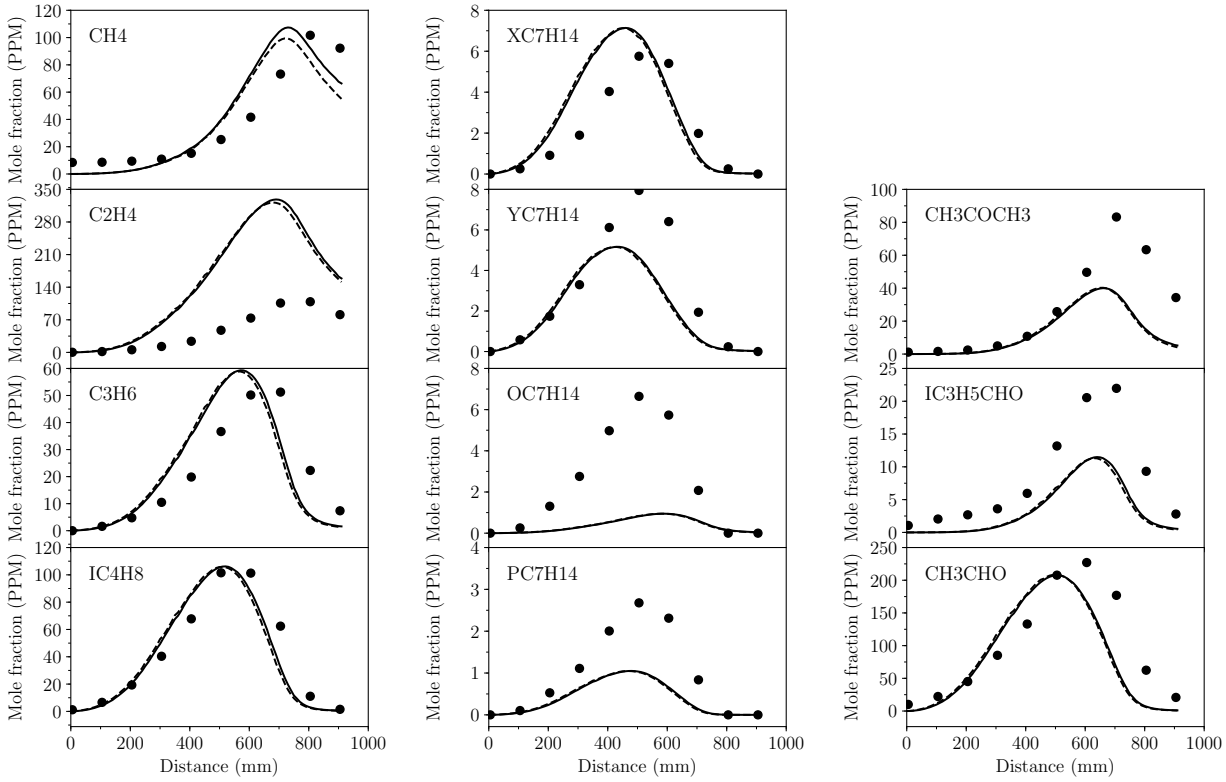

Figure 28: Evolution of intermediate species in the oxidation of TRF91-30 and ethanol mixture. Symbols are experiment results, curves are modelling results by the original Mehl model [10] (solid lines) and the adjusted model (dashed lines).

3.4.3. Implications for gasoline design

We end this paper by relating its findings to those of two works undertaken by the group [4, 58]. Foong et al. [4] undertook a large set of Research and Motor Octane Number tests, and found that more paraffinic and aromatic gasoline surrogates respectively tended to exhibit octane synergism and antagonism with ethanol. The synergism and antagonism of iso-octane and toluene were very clear, with Yuan et al. [6] presenting polynomials that quantify these variations. The study of Foong et al. [58] then compared the autoignition timing from two-zone modelling of the octane rating engine with the Andrae model [62] to that measured in the octane rating engine itself across a range

of PRF/ethanol and TRF/ethanol mixtures. This work was, however, unable to reproduce the measured trends in autoignition timing.

The present work showed that a gasoline surrogate model that sufficiently accounts for the oxidation of toluene is currently lacking in the literature. Accurate modelling of such interactions is required for a gasoline surrogate model to capture the synergism and antagonism in the octane blending of gasoline and ethanol, and thus has significant implications for the design of advanced, low emission gasolines.

4. Conclusions

This paper presented a study of the oxidation of iso-octane, ethanol, toluene and their mixtures in a pressurised flow reactor operating at 900-930 K, 10 bar and an equivalence ratio of 0.058. Detailed species profiles were measured along the length of the reactor and modelled using existing kinetic models from the literature.

The existing models were found to reproduce the measured oxidation of iso-octane, ethanol, their mixtures, as well as that of PRF91 and PRF91/ethanol mixtures. This included the fuel consumption, CO formation, and evolution of major intermediates, namely iso-butylene for iso-octane and acetaldehyde for ethanol. Improvement was nevertheless needed for modelling oxygenates and C_7 olefins for iso-octane, ethylene for ethanol, as well as the conversion of CO to CO_2.

Furthermore, most existing models for toluene did not reproduce the experiments at these test conditions. Other than the models by Metcalfe et al. [15] and Zhang et al. [19], all models significantly over-estimated the oxidation reactivity of toluene, which in turn led to significant disagreement in the modelling of toluene-containing mixtures.

Adjustment was therefore made to the rate constants of selected reactions in the toluene model. However, this adjusted model, whilst more accurately reproducing the oxidation of neat toluene, did not significantly improve the modelling of toluene-containing mixtures. This suggests that further investigations should focus not only on the oxidation of neat toluene, but also on the chemical interactions between toluene and other compounds. Indeed, it is hoped that future improvements in the modelling of toluene-containing mixtures will explain how paraffinic and aromatic fuels respectively tend to exhibit octane synergism and antagonism with ethanol, and thus have significant implications for the design of advanced, low emission gasolines.

Acknowledgements

This research was supported by the Ford Motor Company and the Australian Research Council (DP140100846).

References

[1] C. S. Sluder, D. E. Smith, M. Wissink, J. E. Anderson, T. G. Leone, M. H. Shelby, Effects of octane number, sensitivity, ethanol content, and engine compression ratio on GTDI engine efficiency, fuel economy, and CO_2 emissions, CRC Report No. AVFL-20.

[2] J. E. Leone, Thomas G.and Anderson, R. S. Davis, A. Iqbal, I. Reese, Ronald A., M. H. Shelby, W. M. Studzinski, The effect of compression ratio, fuel octane rating, and ethanol content on spark-ignition engine efficiency, Environ. Sci. Technol. 49 (2015) 10778–10789.

[3] A. J. Stein, R., T. Wallington, An overview of the effects of ethanol-gasoline blends on SI engine performance, fuel efficiency, and emissions, SAE Int. J. Engines 6(1) (2013) 470–487.

[4] T. M. Foong, K. J. Morganti, M. J. Brear, G. da Silva, Y. Yang, F. L. Dryer, The octane numbers of ethanol blended with gasoline and its surrogates, Fuel 115 (2014) 727–739.

[5] J. Badra, A. S. AlRamadan, S. M. Sarathy, Optimization of the octane response of gasoline/ethanol blends, Applied Energy 203 (2017) 778–793.

[6] H. Yuan, Y. Yang, M. J. Brear, T. M. Foong, J. E. Anderson, Optimal octane number correlations for mixtures of toluene reference fuels (TRFs) and ethanol, Fuel 188 (2017) 408–417.

[7] A. S. AlRamadan, S. M. Sarathy, M. Khurshid, J. Badra, A blending rule for octane numbers of PRFs and TPRFs with ethanol, Fuel 180 (2016) 175–186.

[8] H. J. Curran, P. Gaffuri, W. J. Pitz, C. K. Westbrook, A comprehensive modeling study of iso-octane oxidation, Combust. Flame 129 (3) (2002) 253–280.

[9] H. J. Curran, P. Gaffuri, W. J. Pitz, C. K. Westbrook, A Comprehensive Modeling Study of n-Heptane Oxidation, Combust. Flame 114 (1) (1998) 149–177.

[10] M. Mehl, W. J. Pitz, C. K. Westbrook, H. J. Curran, Kinetic modeling of gasoline surrogate components and mixtures under engine conditions, Proc. Combust. Inst. 33 (1) (2011) 193–200.

[11] K. Zhang, C. Banyon, J. Bugler, H. J. Curran, A. Rodriguez, O. Herbinet, F. Battin-Leclerc, C. B'Chir, K. A. Heufer, An updated experimental and kinetic modeling study of n-heptane oxidation, Combust. Flame 172 (2016) 116–135.

[12] N. Atef, G. Kukkadapu, S. Y. Mohamed, M. A. Rashidi, C. Banyon, M. Mehl, K. A. Heufer, E. F. Nasir, A. Alfazazi, A. K. Das, C. K. Westbrook, W. J. Pitz, T. Lu, A. Farooq, C.-J. Sung, H. J. Curran, S. M. Sarathy, A comprehensive iso-octane combustion model with improved thermochemistry and chemical kinetics, Combust. Flame 178 (2017) 111–134.

[13] J. L. Emdee, K. Brezinsky, I. Glassman, A kinetic model for the oxidation of toluene near 1200 K, J. Phys. Chem. 96 (5) (1992) 2151–2161.

[14] S. D. Klotz, K. Brezinsky, I. Glassman, Modeling the combustion of toluene-butane blends, Symp (Int.) Combust. 27 (1) (1998) 337–344.

[15] W. K. Metcalfe, S. Dooley, F. L. Dryer, Comprehensive Detailed Chemical Kinetic Modeling Study of Toluene Oxidation, Energy Fuels 25 (11) (2011) 4915–4936.

[16] W. Yuan, Y. Li, P. Dagaut, J. Yang, F. Qi, Investigation on the pyrolysis and oxidation of toluene over a wide range conditions. I. Flow reactor pyrolysis and jet stirred reactor oxidation, Combust. Flame 162 (1) (2015) 3–21.

[17] W. Yuan, Y. Li, P. Dagaut, J. Yang, F. Qi, Investigation on the pyrolysis and oxidation of toluene over a wide range conditions. II. A comprehensive kinetic modeling study, Combust. Flame 162 (1) (2015) 22–40.

[18] L. Zhang, J. Cai, T. Zhang, F. Qi, Kinetic modeling study of toluene pyrolysis at low pressure, Combust. Flame 157 (9) (2010) 1686–1697.

[19] Y. Zhang, K. P. Somers, M. Mehl, W. J. Pitz, R. F. Cracknell, H. J. Curran, Probing the antagonistic effect of toluene as a component in surrogate fuel models at low temperatures and high pressures. A case study of toluene/dimethyl ether mixtures, Proc. Combust. Inst. 36 (1) (2017) 413–421.

[20] H. Nakamura, D. Darcy, M. Mehl, C. J. Tobin, W. K. Metcalfe, W. J. Pitz, C. K. Westbrook, H. J. Curran, An experimental and modeling study of shock tube and rapid compression machine ignition of n-butylbenzene/air mixtures, Combust. Flame 161 (1) (2014) 49–64.

[21] M. Pelucchi, C. Cavallotti, T. Faravelli, S. J. Klippenstein, H-Abstraction reactions by OH, HO2, O, O2 and benzyl radical addition to O2 and their implications for kinetic modelling of toluene oxidation, PHYS CHEM CHEM PHYS 20 (2018) 10607–10627.

[22] N. M. Marinov, A detailed chemical kinetic model for high temperature ethanol oxidation, Int. J. Chem. Kinet. 31 (3) (1999) 183–220.

[23] J. Li, Experimental and numerical studies of ethanol chemical kinetics, Ph.D. thesis, Princeton University (2004).

[24] P. Dagaut, C. Togb, Experimental and modeling study of the kinetics of oxidation of ethanol−gasoline surrogate mixtures (e85 surrogate) in a jet-stirred reactor, Energy Fuels 22 (5) (2008) 3499–3505.

[25] J. Park, Z. F. Xu, M. C. Lin, Thermal decomposition of ethanol. II. A computational study of the kinetics and mechanism for the H+C2H5OH reaction, J. Chem. Phys. 118 (22) (2003) 9990–9996.

[26] S. Xu, M. C. Lin, Theoretical study on the kinetics for OH reactions with CH3OH and C2H5OH, Proc. Combust. Inst. 31 (1) (2007) 159–166.

[27] Z. F. Xu, J. Park, M. C. Lin, Thermal decomposition of ethanol. III. A computational study of the kinetics and mechanism for the CH3+C2H5OH reaction, J. Chem. Phys. 120 (14) (2004) 6593–6599.

[28] C.-W. Wu, Y.-P. Lee, S. Xu, M. C. Lin, Experimental and Theoretical Studies of Rate Coefficients for the Reaction O(3p) + C2H5OH at High Temperatures, J. Phys. Chem. A 111 (29) (2007) 6693–6703.

[29] G. Mittal, S. M. Burke, V. A. Davies, B. Parajuli, W. K. Metcalfe, H. J. Curran, Autoignition of ethanol in a rapid compression machine, Combust. Flame (2013) 1164–1171.

[30] N. Leplat, P. Dagaut, C. Togb, J. Vandooren, Numerical and experimental study of ethanol combustion and oxidation in laminar premixed flames and in jet-stirred reactor, Combust. Flame 158 (4) (2011) 705–725.

[31] P. Dagaut, M. Reuillon, M. Cathonnet, High Pressure Oxidation of Liquid Fuels from Low to High Temperature. 2. Mixtures of n-Heptane and iso-Octane, Combust. Sci. Technol. 103 (1-6) (1994) 315–336.

[32] Z. Lu, Y. Yang, M. Brear, Oxidation of PRFs and ethanol/isooctane mixtures in a flow reactor and the implication for their octane blending, Proc. Combust. Inst.doi:https://doi.org/10.1016/j.proci.2018.05.134.

[33] W. R. Leppard, The autoignition chemistries of primary reference fuels, olefin/paraffin binary mixtures, and non-linear octane blending, SAE Technical Paper 922325.

[34] M. AlAbbad, T. Javed, F. Khaled, J. Badra, A. Farooq, Ignition delay time measurements of primary reference fuel blends, Combust. Flame 178 (2017) 205–216.

[35] K. Fieweger, R. Blumenthal, G. Adomeit, Self-ignition of S.I. engine model fuels: A shock tube investigation at high pressure, Combust. Flame 109 (4) (1997) 599–619.

[36] R. D. Wilk, D. N. Koert, N. P. Cernansky, Low-temperature carbon monoxide formation as a means of assessing the autoignition tendency of hydrocarbons and hydrocarbon blends, Energy Fuels 3 (3) (1989) 292–298.

[37] G. Vanhove, G. Petit, R. Minetti, Experimental study of the kinetic interactions in the low-temperature autoignition of hydrocarbon binary mixtures and a surrogate fuel, Combust. Flame 145 (3) (2006) 521–532.

[38] M. Yahyaoui, N. Djebali-Chaumeix, P. Dagaut, C. E. Paillard, B. Heyberger, G. Pengloan, Ignition and oxidation of 1-hexene/toluene mixtures in a shock tube and a jet-stirred reactor: Experimental and kinetic modeling study, Int. J. Chem. Kinet. 39 (9) (2007) 518–538.

[39] R. Di Sante, Measurements of the auto-ignition of n-heptane/toluene mixtures using a rapid compression machine, Combust. Flame 159 (1) (2012) 55–63.

[40] P. Dagaut, C. Togb, Experimental and modeling study of the kinetics of oxidation of butanol−n-heptane mixtures in a jet-stirred reactor, Energy Fuels 23 (7) (2009) 3527–3535.

[41] P. Saisirirat, C. Togb, S. Chanchaona, F. Foucher, C. Mounaim-Rousselle, P. Dagaut, Auto-ignition and combustion characteristics in HCCI and JSR using 1-butanol/n-heptane and ethanol/n-heptane blends, Proc. Combust. Inst. 33 (2) (2011) 3007–3014.

[42] P. Dagaut, C. Togb, Oxidation Kinetics of Mixtures of Iso-Octane with Ethanol or Butanol in a Jet-Stirred Reactor: Experimental and Modeling Study, Combust. Sci. Technol. 184 (7-8) (2012) 1025–1038.

[43] F. M. Haas, M. Chaos, F. L. Dryer, Low and intermediate temperature oxidation of ethanol and ethanolPRF blends: An experimental and modeling study, Combust. Flame 156 (12) (2009) 2346–2350.

[44] G. Kukkadapu, K. Kumar, C.-J. Sung, M. Mehl, W. J. Pitz, Autoignition of gasoline surrogates at low temperature combustion conditions, Combust. Flame 162 (5) (2015) 2272–2285.

[45] T. Javed, C. Lee, M. AlAbbad, K. Djebbi, M. Beshir, J. Badra, H. Curran, A. Farooq, Ignition studies of n-heptane/iso-octane/toluene blends, Combust. Flame 171 (2016) 223–233.

[46] A. S. AlRamadan, J. Badra, T. Javed, M. Al-Abbad, N. Bokhumseen, P. Gaillard, H. Babiker, A. Farooq, S. M. Sarathy, Mixed butanols addition to gasoline surrogates: Shock tube ignition delay time measurements and chemical kinetic modeling, Combust. Flame 162 (10) (2015) 3971–3979.

[47] E. Agbro, A. S. Tomlin, M. Lawes, S. Park, S. M. Sarathy, The influence of n-butanol blending on the ignition delay times of gasoline and its surrogate at high pressures, Fuel 187 (2017) 211–219.

[48] S. M. Sarathy, A. Farooq, G. T. Kalghatgi, Recent progress in gasoline surrogate fuels, Prog. Energy Combust. Sci. 65 (2018) 67–108.

[49] S. Dooley, S. H. Won, M. Chaos, J. Heyne, Y. Ju, F. L. Dryer, K. Kumar, C.-J. Sung, H. Wang, M. A. Oehlschlaeger, R. J. Santoro, T. A.

Litzinger, A jet fuel surrogate formulated by real fuel properties, Combust. Flame 157 (12) (2010) 2333–2339.

[50] S. Dooley, S. H. Won, J. Heyne, T. I. Farouk, Y. Ju, F. L. Dryer, K. Kumar, X. Hui, C.-J. Sung, H. Wang, M. A. Oehlschlaeger, V. Iyer, S. Iyer, T. A. Litzinger, R. J. Santoro, T. Malewicki, K. Brezinsky, The experimental evaluation of a methodology for surrogate fuel formulation to emulate gas phase combustion kinetic phenomena, Combust. Flame 159 (4) (2012) 1444–1466.

[51] F. L. Dryer, Chemical kinetic and combustion characteristics of transportation fuels, Proc. Combust. Inst. 35 (1) (2015) 117–144.

[52] S. Benson, Thermochemical Kinetics: Methods for the Estimation of Thermochemical Data and Rate Parameters, Wiley, 1976.

[53] Z. Lu, J. Cochet, N. Leplat, Y. Yang, M. J. Brear, A high-pressure plug flow reactor for combustion chemistry investigations, Meas. Sci. Technol. 28 (2017) 105902–105915.

[54] J. T. Scanlon, D. E. Willis, Calculation of Flame Ionization Detector Relative Response Factors Using the Effective Carbon Number Concept, J. Chromatogr. Sci. 23 (8) (1985) 333–340.

[55] A. D. Jorgensen, K. C. Picel, V. C. Stamoudis, Prediction of gas chromatography flame ionization detector response factors from molecular structures, Anal. Chem. 62 (7) (1990) 683–689.

[56] H. Yuan, Octane Blending and Oxidation Chemistry of Ethanol-Hydrocarbon Mixtures, Ph.D. thesis, The University of Melbourne (2018).

[57] Z. Lu, Investigation of autoignition chemistry of ethanol and primary reference fuels in a pressurised flow reactor, Ph.D. thesis, The University of Melbourne (2018).

[58] T. M. Foong, M. J. Brear, K. J. Morganti, G. da Silva, Y. Yang, F. L. Dryer, Modeling End-Gas Autoignition of Ethanol/Gasoline Surrogate Blends in the Cooperative Fuel Research Engine, Energy Fuels 31 (3) (2017) 2378–2389.

[59] D. B. Lenhert, D. L. Miller, N. P. Cernansky, K. G. Owens, The oxidation of a gasoline surrogate in the negative temperature coefficient region, Combust. Flame 156 (3) (2009) 549–564.

[60] CHEMKIN-PRO 15131, Reaction Design: San Diego.

[61] F. L. Dryer, F. M. Haas, J. Santner, T. I. Farouk, M. Chaos, Interpreting chemical kinetics from complex reactionadvectiondiffusion systems: Modeling of flow reactors and related experiments, Prog. Energy Combust. Sci. 44 (2014) 19–39.

[62] J. C. G. Andrae, Development of a detailed kinetic model for gasoline surrogate fuels, Fuel 87 (1011) (2008) 2013–2022.

[63] C.-W. Zhou, Y. Li, E. O'Connor, K. P. Somers, S. Thion, C. Keesee, O. Mathieu, E. L. Petersen, T. A. DeVerter, M. A. Oehlschlaeger, G. Kukkadapu, C.-J. Sung, M. Alrefae, F. Khaled, A. Farooq, P. Dirrenberger, P.-A. Glaude, F. Battin-Leclerc, J. Santner, Y. Ju, T. Held, F. M. Haas, F. L. Dryer, H. J. Curran, A comprehensive experimental and modeling study of isobutene oxidation, Combust. Flame 167 (2016) 353–379.

[64] F. L. Dryer, K. Brezinsky, A Flow Reactor Study of the Oxidation of n-Octane and Iso-Octane, Combust. Sci. Technol. 45 (3-4) (1986) 199–212.

[65] J.-S. Chen, T. A. Litzinger, H. J. Curran, The Lean Oxidation of Iso-Octane in the Intermediate Temperature Regime at Elevated Pressures, Combust. Sci. Technol. 156 (1) (2000) 49–79.

[66] P. Dagaut, M. Reuillon, M. Cathonnet, High Pressure Oxidation of Liquid Fuels From Low to High Temperature. 1. n-Heptane and iso-Octane., Combust. Sci. Technol. 95 (1-6) (1993) 233–260.

[67] X. He, S. M. Walton, B. T. Zigler, M. S. Wooldridge, A. Atreya, Experimental investigation of the intermediates of isooctane during ignition, Int. J. Chem. Kinet. 39 (9) (2007) 498–517.

[68] D. J. M. Ray, D. J. Waddington, Gas phase oxidation of alkenes-Part II. The oxidation of 2-methylbutene-2 and 2,3-dimethylbutene-2, Combust. Flame 20 (3) (1973) 327–334.

[69] D. J. M. Ray, R. Ruiz Diaz, D. J. Waddington, Gas-phase oxidation of butene-2: The role of acetaldehyde in the reaction, Symp (Int.) Combust. 14 (1) (1973) 259–266.

[70] A. V. Joshi, H. Wang, Master equation modeling of wide range temperature and pressure dependence of CO + OH → products, Int. J. Chem. Kinet. 38 (1) (2006) 57–73.

[71] C. L. Barraza-Botet, S. W. Wagnon, M. S. Wooldridge, Combustion Chemistry of Ethanol: Ignition and Speciation Studies in a Rapid Compression Facility, J. Phys. Chem. A 120 (38) (2016) 7408–7418.

[72] G. da Silva, J. W. Bozzelli, Kinetic modeling of the benzyl+HO2 reaction, Proc. Combust. Inst. 32 (1) (2009) 287–294.

[73] D. L. Baulch, C. J. Cobos, R. A. Cox, P. Frank, G. Hayman, T. Just, J. A. Kerr, T. Murrells, M. J. Pilling, J. Troe, R. W. Walker, J. Warnatz, Evaluated Kinetic Data for Combustion Modeling. Supplement I, J. Phys. Chem. Ref. Data 23 (6) (1994) 847–848.